# EUMETSAT Satellite Application Facility on Climate Monitoring


# Algorithm Theoretical Baseline Document

# Spectrally Resolved Solar Surface Irradiance SRI

DOI:10.5676/EUMETSAT_SAF_CM/CLAAS/V001

**Spectrally Resolved Irradiance** **CM-107**

Reference Number: SAF/CM/DWD/ATBD/SRI
Issue/Revision Index: 1.2
Date: 16.10.2013

## Document Signature Table

| | Name | Function | Signature | Date |
|---|---|---|---|---|
| Author | Richard Müller | CM SAF scientist | | 25/04/2012 |
| Author | T. Behrendt | PhD | | 25/04/2012 |
| Editor | Rainer Hollmann | Science Coordinator | | 25/04/2012 |
| Approval | | CM SAF Steering Group | | 16/04/2013 |
| Release | Martin Werscheck | Project Manager | | 16/04/2013 |

## Distribution List

| Internal Distribution | |
|---|---|
| Name | No. Copies |
| DWD Archive | 1 |
| CM SAF Team | 1 |

| External Distribution | | |
|---|---|---|
| Company | Name | No. Copies |
| PUBLIC | | 1 |

## Document Change Record

| Issue/ Revision | Date | DCN No. | Changed Pages/Paragraphs |
|---|---|---|---|
| 1.0 | 05/11/2010 | SAF/CM/DWD/ATBD/SRI | Version presented to PCR-4 review |
| 1.1 | 25/04/2012 | SAF/CM/DWD/ATBD/SRI | Implement of changes due to PCR-4 review |
| 1.2 | 16/10/2013 | SAF/CM/DWD/ATBD/SRI | Correction of DOI-number |

## Applicable Documents

| **Reference** | **Title** | **Code** |
|---|---|---|
| AD 1 | CM SAF Product Requirements Document | SAF/CM/DWD/PRD/2.1 |

## Reference Documents

| **Reference** | **Title** | **Code** |
|---|---|---|
| RD.1 | ATBD Meteosat (MVIRI) Climate Data Set of SIS,SID and CAL : MVIRI_HEL | SAF/CM/DWD/PUM/MVIRI_HEL/1.1 |

## Table of Contents

## Table of Figures

# 1 The EUMETSAT SAF on Climate Monitoring (CMSAF)

The importance of climate monitoring with satellites was recognized in 2000 by EUMETSAT Member States when they amended the EUMETSAT Convention to affirm that the EUMETSAT mandate is also to “contribute to the operational monitoring of the climate and the detection of global climatic changes". Following this, EUMETSAT established within its Satellite Application Facility (SAF) network a dedicated centre, the SAF on Climate Monitoring (CM SAF, http://www.cmsaf.eu).
The consortium of CM SAF currently comprises the Deutscher Wetterdienst (DWD) as host institute, and the partners from the Royal Meteorological Institute of Belgium (RMIB), the Finnish Meteorological Institute (FMI), the Royal Meteorological Institute of the Netherlands (KNMI), the Swedish Meteorological and Hydrological Institute (SMHI), the Meteorological Service of Switzerland (MeteoSwiss), and the Meteorological Service of the United Kingdom (UK MetOffice). Since the beginning in 1999, the EUMETSAT Satellite Application Facility on Climate Monitoring (CM SAF) has developed and will continue to develop capabilities for a sustained generation and provision of Climate Data Records (CDR’s) derived from operational meteorological satellites.
In particular the generation of long-term data sets is pursued. The ultimate aim is to make the resulting data sets suitable for the analysis of climate variability and potentially the detection of climate trends. CM SAF works in close collaboration with the EUMETSAT Central Facility and liaises with other satellite operators to advance the availability, quality and usability of Fundamental Climate Data Records (FCDRs) as defined by the Global Climate Observing System (GCOS). As a major task the CM SAF utilizes FCDRs to produce records of Essential Climate Variables (ECVs) as defined by GCOS. Thematically, the focus of CM SAF is on ECVs associated with the global energy and water cycle.

Another essential task of CM SAF is to produce data sets that can serve applications related to the new Global Framework of Climate Services initiated by the WMO World Climate Conference-3 in 2009. CM SAF is supporting climate services at national meteorological and hydrological services (NMHSs) with long-term data records but also with data sets produced close to real time that can be used to prepare monthly/annual updates of the state of the climate. Both types of products together allow for a consistent description of mean values, anomalies, variability and potential trends for the chosen ECVs. CM SAF ECV data sets also serve the improvement of climate models both at global and regional scale.
As an essential partner in the related international frameworks, in particular WMO SCOPE-CM (Sustained COordinated Processing of Environmental satellite data for Climate Monitoring), the CM SAF - together with the EUMETSAT Central Facility, assumes the role as main implementer of EUMETSAT’s commitments in support to global climate monitoring. This is achieved through:

- Application of highest standards and guidelines as lined out by GCOS for the satellite data processing,
- Processing of satellite data within a true international collaboration benefiting from developments at international level and pollinating the partnership with own ideas and standards,
- Intensive validation and improvement of the CM SAF climate data records,
- Taking a major role in data set assessments performed by research organisations such as WCRP (World Climate Research Program). This role provides the CM SAF with deep contacts to research organizations that form a substantial user group for the CM SAF CDRs,

- Maintaining and providing an operational and sustained infrastructure that can serve the community within the transition of mature CDR products from the research community into operational environments.

A catalogue of all available CM SAF products is accessible via the CM SAF webpage, www.cmsaf.eu. Here, detailed information about product ordering, add-on tools, sample programs and documentation is provided.

## 2 Introduction

The solar surface irradiance consists of a diffuse fraction and a direct fraction. The diffuse fraction of the surface irradiance is defined as the solar radiation that has undergone scattering in the atmosphere. The direct irradiance is the flux reaching a horizontal unit of the earth's surface in the solar wavelength region from the direction of the sun without being scattered. Both quantities are expressed in W/m². The spectrally resolved solar surface irradiance (SRI) is the solar surface irradiance (direct and diffuse component) given at specific wavelengths ore wavelength bands, see Figure 2–1 for illustration of the solar spectrum.

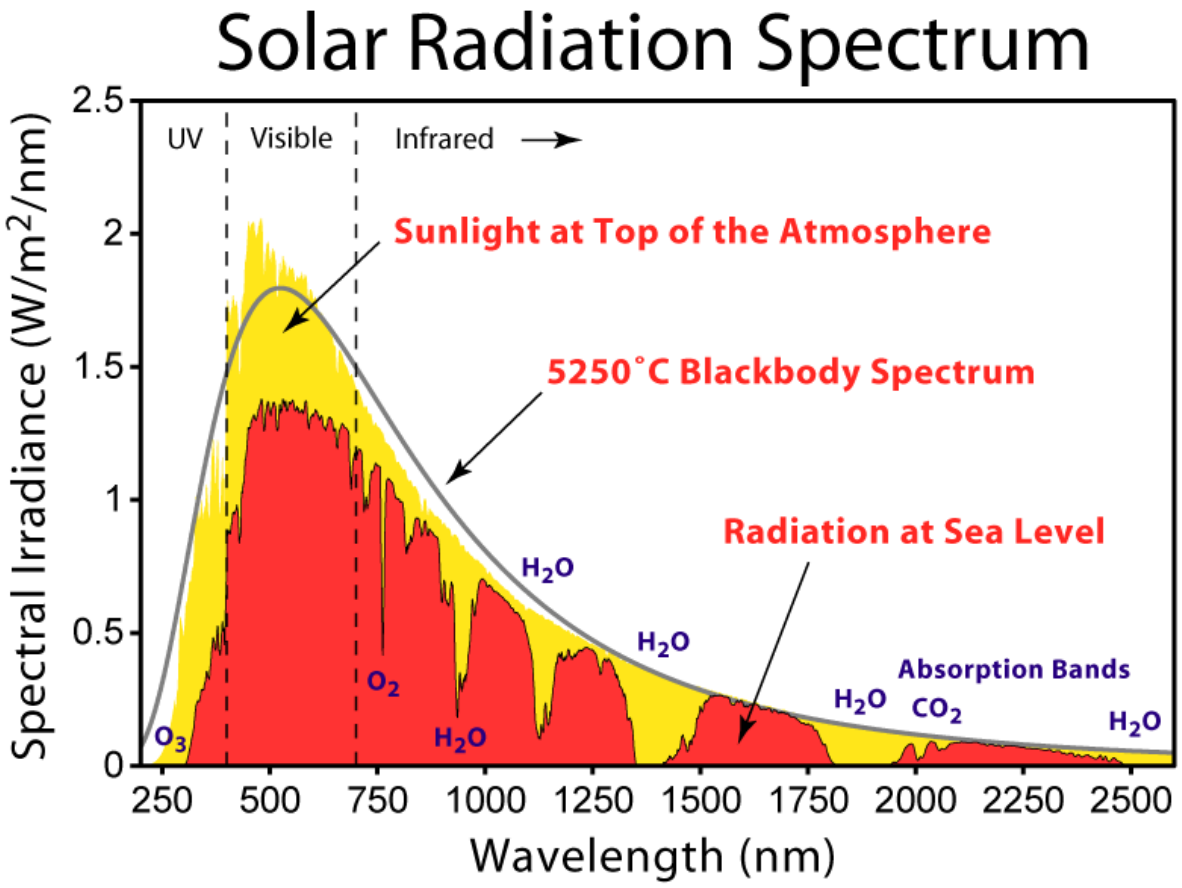


Figure 2–1: The figure illustrates the solar spectrum at top of atmosphere and the surface. Especially the water absorption bands leads to large gaps in the solar surface irradiance. Hence, different amounts of water vapour do affect the radiation spectrum significantly.

Accurate information on spectrally resolved irradiance is important for

- the prediction of energy yield, the planning, monitoring and system design of thin solar cells, tandem and triple-junction PV cells (see Figure 2–2 for example).
- the analysis and understanding of the climate system in particular processes that are spectrally sensitive like photosynthesis or absorption of irradiance by the Earth's surface.
- the prediction of energy yield of multi-junction cells for concentrating PV modules, which are very sensitive to the solar spectrum.

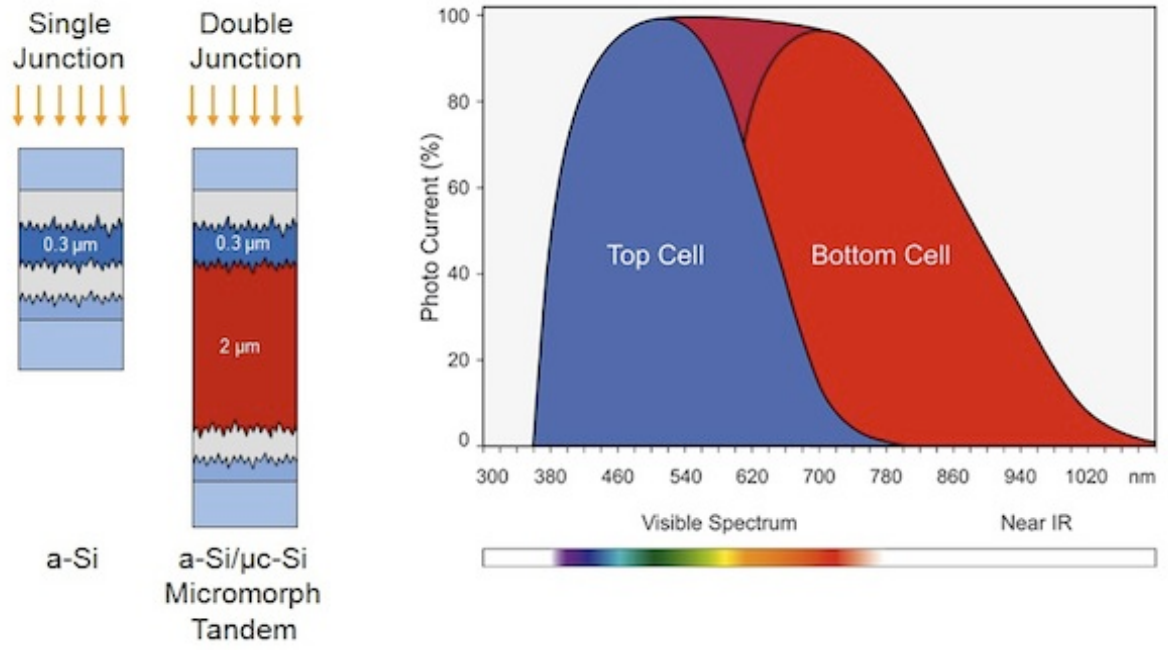


Figure 2–2: Example of a tandem solar cell. The spectral sensitivity (right hand) can be significantly increased by combination of two cells to a tandem cell (left hand). However, this leads to a higher sensitivity of the PV output on the spectra e.g. as induced by variations in water vapour, as the extended wavelength regions covers water vapour absorption bands.

Almost no well-maintained ground measurements of spectrally resolved irradiance covering 300-1500nm exist in Europe and to our knowledge any in Africa and over the ocean. As geostationary satellites enable the retrieval of area-wide broadband solar surface irradiance in high spatial and temporal resolution with good accuracy it is likely that these satellites constitute also an observational source for spectrally resolved irradiance.
In the last years, CM SAF has successfully extended well-established methods used within the Solar Energy community (e.g., Skartveith et al., 1998, Posselt et al. 2012) to include the information on the atmospheric composition nowadays available from the new generation of satellites (e.g., SCIAMACHY, MSG). One important extension of the MAGICSOL (MAGIC SOLar irradiance) algorithm (Mueller et al.. 2009), which has also been used for the production of the CM SAF MVIRI SIS and SID data sets, is that it employs detailed aerosol information instead of turbidity maps. The clear sky irradiance is completely based on Radiative Transfer Modelling. Finally, a correction of spectral cloud effect enables the retrieval of spectrally resolved irradiance with MAGICSOLs, the spectral version of MAGICSOL.

Long time series are needed for climate monitoring and analysis. For this reason there is a need to employ the satellite information of the first generation of Meteosat satellites (Meteosat-2 to Meteosat-7) to generate climate information. The MVIRI instrument onboard

the Meteosat First Generation satellites is equipped with 3 channels: a broadband channel in the visible, a channel in the Infrared, and a water vapour channel.
The second generation of Meteosat satellites is equipped with the Spinning Enhanced Visible and InfraRed Imager (SEVIRI) and the Geostationary Earth Radiation Budget (GERB) instrument. The GERB instrument is a visible-infrared radiometer for earth radiation budget studies. It provides accurate measurements of the shortwave (SW) and longwave (LW) components of the radiation budget at the top of the atmosphere. SEVIRI employs twelve spectral channels, which provide more information of the atmosphere compared to its forerunner. Several retrieval algorithms have been developed in order to use the additional information gained by the improved spectral information of MSG mainly for now-casting applications. However, these algorithms can not be applied to the MVIRI instrument onboard the Meteosat First Generation satellites as they use spectral information that is not provided by MFG (NWC SAF cloud algorithm, CM SAF radiation algorithm).
MVIRI is a passive imaging radiometer with three spectral chances a visible channel covering 500-900 nm, and infra-red channel covering 5.7-7.1 microns and 10.5-12.5 microns. MVIRI comes with a spatial resolution of 2.5km for the visible and 5km for the IR channels, sub-satellite point respectively.
Hence, in order to be able to provide a long time series covering more than 20 years there is a need for a specific climate algorithm that can be applied to the satellites from the Meteosat First and Second Generation. Moreover, the retrieved climate variable must have climate quality.

# 3 Algorithm Overview SRI

The MAGICSOL (MAGIC SOLar irradiance) method, a combination of a climate Heliosat (HELIOSATellite) version (Hammer et al. 2003) and the Magic Global Irradiance Code - MAGIC (Mueller et al., 2009) does meet the above mentioned requirements. The method provides the spectrally resolved solar surface irradiance on a horizontal plane.
The applied MAGICSOLs method needs only the broadband visible channel as satellite information and can therefore be applied to MFG and across different satellite generations.
Hence, the MAGICSOLs method has not only the power to provide long time series of ECVS, but also to provide ECVs, which cover the complete geostationary ring.

The Heliosat method, which is well established in the solar energy community, is the basis of the MAGICSOLs method for clouds. However, modifications of the original Heliosat method are needed to meet the requirements to generate a Climate Data Record and to provide spectrally resolved irradiance
The spectral effect of clouds is treated by spectral correction of the broadband effective cloud albedo performed by the application of RTM based LUTs. Figure 3–1 illustrates the functional principle of a Look-Up-Table (LUT). Figure 3–2 and Figure 3–3 provide a functional diagram of the algorithms, whereby Figure 3–3 includes independencies to other CM SAF data sets.

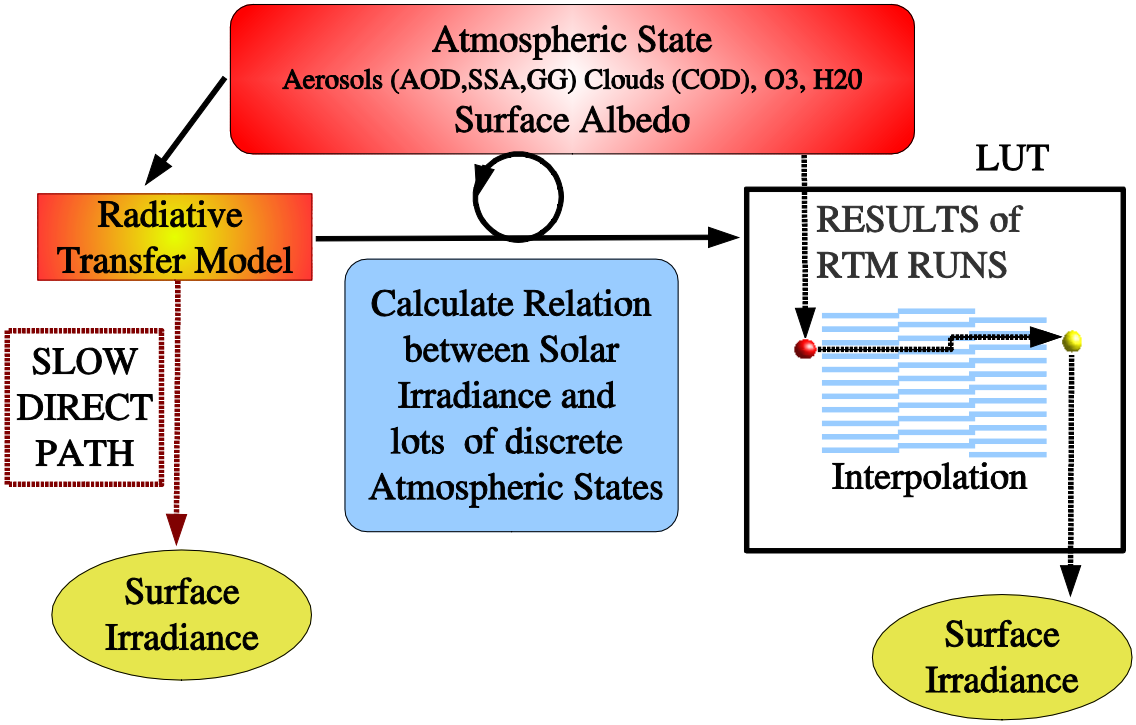


Figure 3–1: The relation of the transmission to a manifold of atmospheric states is pre-calculated with a radiative transfer model (RTM) and saved in a look-up table (LUT). Once, the LUT has been computed the transmittance for a given atmospheric state can be extracted from the LUT for each satellite pixel and time.

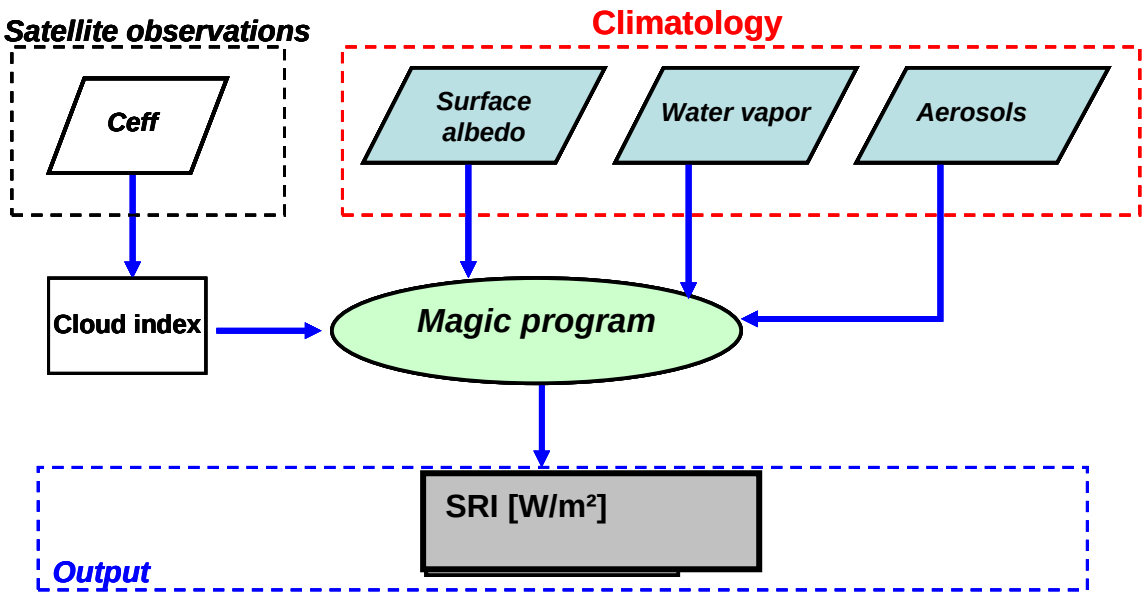


Figure 3–2: Diagram of the interface of MAGIC to the atmospheric input and the satellite observations, Ceff stands for the dark offset corrected and normalised Counts.

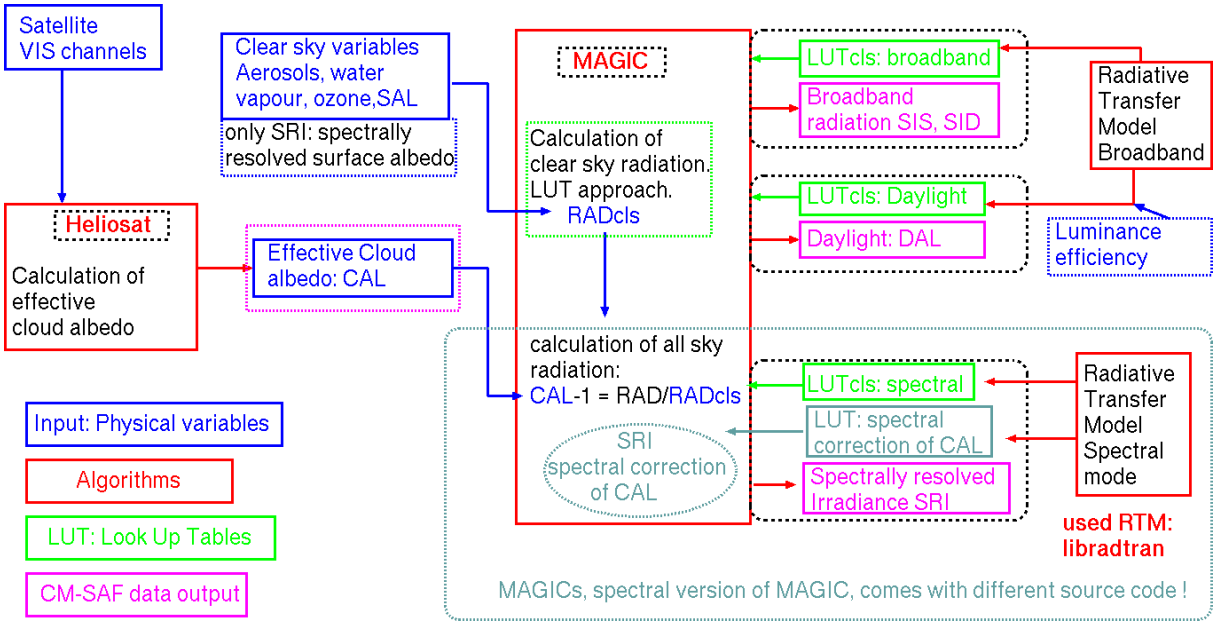


**Figure 3–3:** Functional diagram of the MAGICSOL algorithm for the calculation of spectrally resolved irradiance including independency with other CM SAF radiation data sets. The retrieval of the effective cloud albedo is the basis input for all surface irradiance data sets. For the spectral resolved irradiance a spectral correction of the broadband effective cloud albedo is applied, which is not needed for daylight and broadband irradiance. The core of the algorithms is the MAGIC algorithms. Dependent on the used Look-Up-Table MAGIC enables the calculation of broadband radiation and daylight. The MAGIC version for the spectral resolved irradiance MAGICs comes with the same approach concerning the physics, but the source code is optimised for the treatment of spectral bands and is therefore different to that of the broadband MAGIC code applied to derive daylight and broadband solar surface irradiance.

# 4 Theoretical Description

## 4.1 Physical Baseline

The pre-dominant effect on the solar irradiance spectra is related to absorption by atmospheric components and Rayleigh scattering. The effect of Mie-Scattering on the spectra is in comparison with these effects rather weak.
This in turn suggests the separation of the effects of clouds, which is predominantly a Mie-scattering effect, from the clear sky effect on spectrally resolved solar irradiance.
The broadband cloud effect on the solar irradiance can be well defined with the effective cloud albedo derived with the established, accurate and fast MAGICSOL method Posselt et al. 2012. The problem for clouds breaks therefore down to the spectral correction of the broadband cloud albedo for the rather weak Mie scattering effect on the spectrum.
For these corrections a simple look-up table can be calculated with radiative transfer models that converts the broadband to the spectral cloud albedo.
The remaining issue is related to the estimation of the clear sky spectrum. The clear sky spectrum can be derived with a hybrid eigenvector approach discussed in detail in Mueller et al (2009). This approach has been originally developed for the broadband irradiance but is extended to spectral bands utilizing its complete strength. In detail all equations given in Mueller et. al (2009) are applied to wavelength bands.
For this purpose the radiative transfer model libRadtran has been applied for the calculation of the basis look-up table for the different spectral bands. LibRadtran is a collection of C and Fortran functions and programs for calculation of solar and thermal radiation in the Earth's atmosphere (A. Kylling and B. Mayer, http:// www.libradtran.org). It has (also) been validated by comparison with other models (Koepke et al. 1998, vanWeele et al. 2000}, and radiation measurements (Mayer et al. 1997)

LibRadtran offers the possibility of using the correlated-k approach of Kato et al. (1999). The correlated-k method is developed to compute the spectral transmittance (hence the spectral fluxes) based on grouping of gaseous absorption coefficients. The main idea is to benefit from the fact that the same value of the absorption coefficient k is encountered many times over a given spectral interval. Thus, the computing time can be decreased by eliminating the redundancy, grouping the values of k, and performing the transmittance calculation only once for a given value of k. 32 Kato bands are available in the solar spectrum.
For the retrieval of clear sky spectral irradiance $SRI_{cls}$ radiative transfer model (RTM) simulations have been conducted for the irradiances and stored in LUTs (Figure 3–1). Throughout the ATBD $_{cls}$ stands for clear sky. A LUT is a data structure used to replace the time-consuming RTM computation with a simpler and faster interpolation operation within discrete pre-computed RTM results.
The basis LUT has been calculated for the 32 Kato bands, by application of the approach of Mueller et al. (2009) for each of the Kato wavelength bands.
In order to consider the cloud effect on $SRI_{cls}$ the well established Heliosat relations Hammer et al. (2003) are employed and adapted to the wavelength bands, which are outlined in the next paragraph; please see section 4.2.2 for further details.

**Relation of effective cloud albedo to solar surface irradiance:**
The effective cloud albedo is related to the solar irradiance via the clear sky index. The clear sky index, k, is defined as

$$K^{wb} = SIS^{wb} / SIS^{wb}_{CLS}.$$

Here $SIS^{wb}_{CLS}$ is the solar irradiance for cloud free skies and $SIS^{wb}$ the solar surface irradiance in the Kato wavelengths bands, respectively .The relation between the effective cloud albedo CAL described in detail in and the clear sky index is mainly given by:

$$K^{wb} = 1 - CAL^{wb}.$$

Here $K^{wb}$ and $CAL^{wb}$ are the clear sky index and the effective cloud albedo in the Kato wavelength bands, respectively.
This relation is defined by physics, in detail by the law of energy conservation (Dagested, 2005). However, above a CAL value of 0.8 empirical corrections are needed as a consequence of the effect of optical thick convective clouds. The applied corrections are described in detail in section 4.2.2 and Hammer et al (2003). With the knowledge of the effective cloud albedo, the surface solar irradiance can be derived using the above formulas.
The spectrally resolved effective cloud albedo is derived from the broadband CAL with a spectral correction based on radiative transfer modelling.

## 4.2 Description of the Algorithm

### 4.2.1 Clear Sky model: The GNU-MAGIC approach for the retrieval of solar irradiance

The physical basis of the algorithm is described in Müller et. al (2009) and R. Müller et al. (2003). The MAGIC approach is applied to spectral bands and used to retrieve the spectrally resolved irradiance $SIS^{wb}_{cls}$ It combines the hybrid-eigenvector hybrid approach for the calculation of the clear sky irradiances with the well established Heliosat relations (see section 4.2.2) for the consideration of the cloud effect. The MAGIC method for the retrieval of the spectrally resolved clear sky irradiance is described in this section while in the following section the treatment of the cloud effect on the clear sky spectra is discussed.
The MAGIC code is based on the radiative transfer model calculations, following a hybrid look-up-table approach. The MAGIC code includes a basic clear-sky look-up-table (LUT), surface albedo map, water vapour climatology and aerosol climatology. The basic clear-sky LUT consists of radiative transfer model results for aerosols with different aerosol optical thickness, single scattering albedo, and asymmetry parameter. Fixed values for water vapour, ozone and surface albedo have been used for the calculation of the basis LUT: 15

kg/m$^2$ for water vapour column, 345 DU of ozone, and a surface albedo of 0.2. The basis LUT contains the results for all 32 Kato bands. The effect of the solar zenith angle on the transmission, hence the surface solar irradiance, is considered by the use of the Modified Lambert Beer (MLB) function (Mueller, 2004). The effects of variations in water vapour and surface albedo relative to the fixed values used in the calculation of the basis LUT are corrected using the correction formulas and parameterizations. The databases in the MAGIC code can be updated and replaced with instantaneous measurements without changing the basic LUT and the code. Therefore the MAGIC code is fast, robust and suitable for operational algorithms.

The input parameters of the MAGIC code are date, time, solar zenith angle, latitude, longitude, effective cloud albedo (cloud index), water vapour column density, aerosol optical thickness and single scatter albedo for aerosols. The output of the MAGICs code are the clear-sky and optionally the all sky solar irradiances in the 0.2-4.0 µm wavelength region, either the broadband sum or the spectral resolved irradiance. The asymmetry parameter for the aerosol scattering phase function is also fixed at 0.7 in the current version of the MAGIC code. The extraterrestrial total solar irradiance is 1366 W/m$^2$ and adjusted according to the earth-sun distance. The relation between the effective cloud albedo CAL and the clear sky index k is already included in the MAGIC code. More details about the MAGIC code are described by Mueller et al. (2004, 2009)

The RTM libRadtran (Mayer and Kylling, 2005) was used for the generation of the basis LUT. RTM calculations were performed for 32 spectral bands between 250 and 3600 nm for numerous states of aerosols. Several types of aerosols were included (Hess et al., 1998). Increase in the computing performance has been achieved by the use of Modified Lambert Beer (MLB) functions (Müller et al., 2004) and the implementation of hybrid eigenvector LUTs (Müller et al., 2009). The MLB relation works very well for the spectral resolved data, see Figure 4–1 as an example.

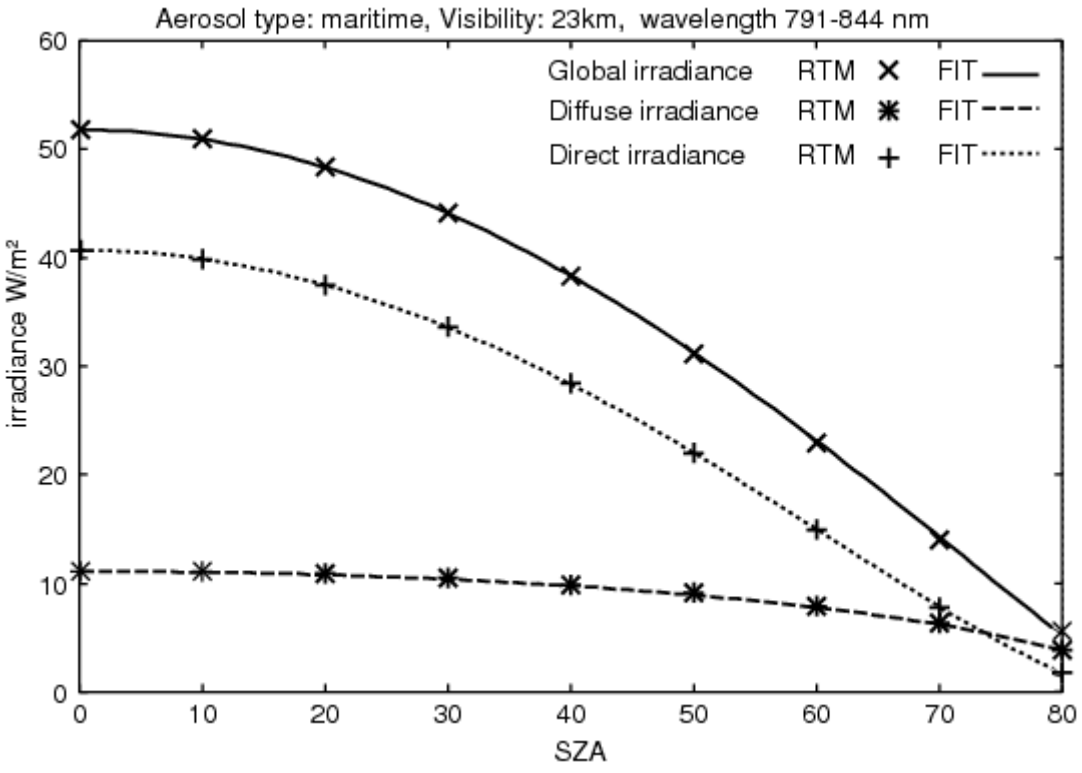


Figure 4–1: Example, the MLB function applied to the spectral Kato band 818. The solar surface irradiance in this band gained from the MLB function (lines) is compared to explicit RTM runs (crosses), please the appendix for further details on the MLB function.

Employing the MAGIC eigenvector hybrid LUT approach the clear sky solar irradiance is calculated in a first step for the given atmospheric conditions and each specific wavelength band. The atmospheric conditions cover different values for water vapour, ozone, aerosol optical depth, aerosol single scattering albedo and asymmetry parameter, and surface albedo.

Within the basic LUT the solar irradiance for the actual aerosol state is derived by linear interpolation between the pre-calculated solar irradiance values associated to different aerosol states for fixed water vapour amount of 15 mm, an ozone content of 345 DU and a surface albedo of 0.2 for each wavelength band. Deviations in water vapour, ozone and the surface albedo from the values assumed for the creation of the LUT are afterwards corrected by application of Eq. 4-1 and Eq. 4-2. Please see Figure 4–2 for a flow diagram of the scheme.

$$SIS^{wb}_{COR} = SIS^{wb}_{LUT} + \Delta SIS^{wb}_{H20} * \cos(SZA)^{a} \qquad \text{Eq. 4-1}$$

The same equation is applied for ozone in a second step.

$SIS^{wb}_{LUT}$ is the solar surface irradiance at the specific wavelength band *wb* derived from the basis LUT for fixed water vapour amount of 15mm, $SIS^{wb}_{COR}$ is the solar surface irradiance corrected for the actual (real) water vapour amount at the specific band, and SZA is the solar zenith angle. $\Delta\ SIS^{wb}_{H20}$ is the difference between $SIS^{wb}$ for the 15 kg/m2 water vapour and the real amount of water vapour, for SZA=0 and a fixed standard atmosphere defined by rural aerosol type with an AOD of 0.2, a surface albedo of 0.2 and 345 DU ozone. $\Delta\ SIS^{wb}_{H20}$ depends on the amount of water vapour. It is pre-calculated for 18 water vapour amounts within the range of 2.5 to 70 mm (the interpolation grid corresponds to those illustrated in Figure 4–6. The algorithm uses the appropriate $\Delta SIS^{wb}_{H20}$ value for the specific pixel and time. The exponent is 0.88. The validity of this formula was verified by comparison with radiative transfer model results. A corresponding equation is used for the ozone correction.

Eq. 4-2 gives the correction of deviations in the surface albedo relative to the standard value used in the basis LUT. Here, $SAL^{wb}$ is the surface albedo and $SIS^{wb}_{COR}$ is the $SIS^{wb}$ retrieved from the LUT, but already corrected for the water vapour and ozone effect.

$$SIS^{wb} = SIS^{wb}_{COR} * (0.98 + 0.1 * SAL^{wb}) \qquad \text{Eq. 4-2}$$

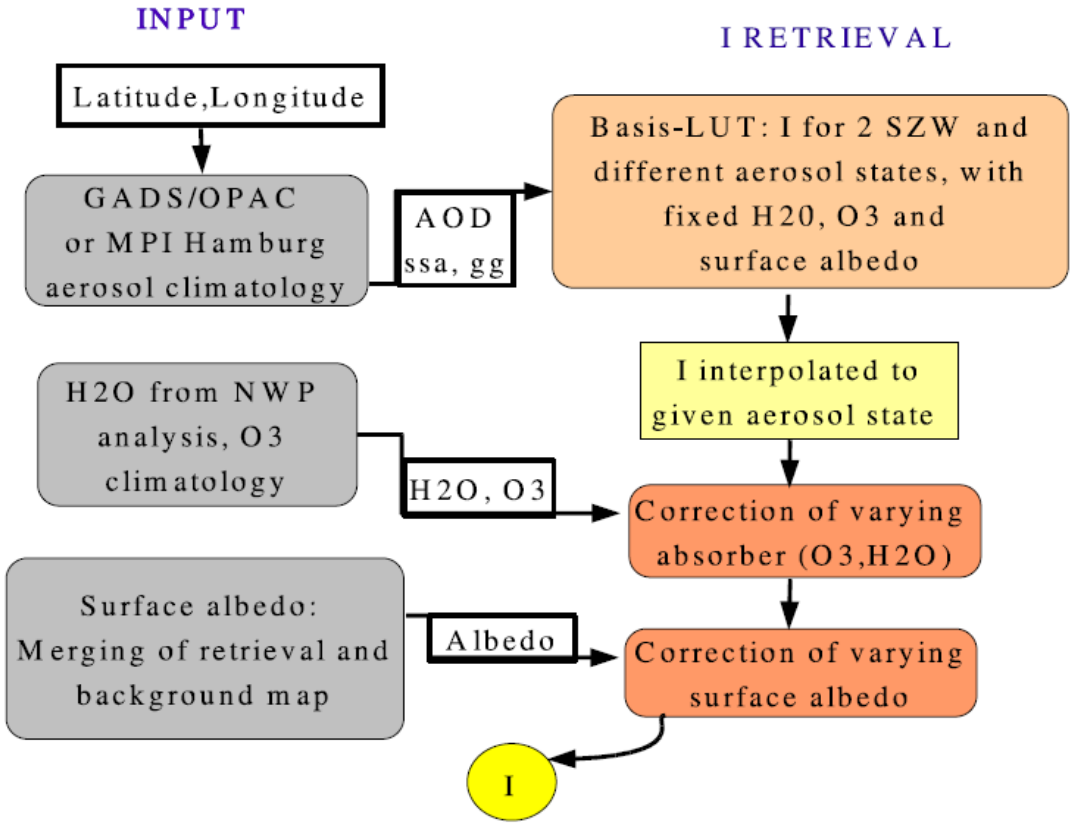


Figure 4–2: Flow-diagram of the clear sky LUT approach for SIS. NWP: Numerical Weather Prediction.

The clear sky method (Müller et al. 2009) has been applied for the retrieval of a CM SAF climate data set including validation (Posselt et al. 2012).

### 4.2.2 Treatment of the cloud effect

The broadband cloud transmission is calculated from the effective cloud albedo derived with the MAGICSOL method. The effective cloud albedo is defined as the normalised difference between the all sky and clear sky reflection in the visible observed by the satellite. The deviation of the actual reflection of the pixel from the clear sky reflection is a measure of the cloudiness. The brighter the pixel the more or thicker clouds are present. The effective cloud albedo is a measure of the cloud effect on the Earth's solar radiation budget.
The MAGICSOL algorithm uses reflection measurements given as normalized digital counts to determine the effective cloud albedo, also called cloud index (Cano et al., 1986; Beyer et al., 1996; Hammer et al., 2003). A clear sky model is used to calculate the solar surface irradiance based on the retrieved effective cloud albedo.
Basis of the Heliosat method are the rectified digital pixel counts of the visible Meteosat channel (High Resolution Visible). The respective data are called *"Rectified Image Data*" and provided by Eumetsat (EUM TD 06). No information from other channels is used. The first step in the Heliosat method is the retrieval of the effective cloud albedo (cloud index).

Thereby, the changes in the reflective properties of the clouds due to different insulation angles during the day and year are accounted for by a normalization with the sun elevation ($\cos(\Theta_z)$ - cosine of the sun's zenith angle) and a correction for the sun-earth distance f.

Furthermore, the measured count value D is reduced by the dark offset $D_0$, which is a satellite specific value obtained by looking into dark space. Values below the dark offset are, thus, assumed to be zero.

$$\rho = \frac{D - D_0}{f \cos(\Theta_z)} \qquad \text{Eq. 4-3}$$

Here, D is the observed digital count including the dark offset of the satellite instrument. The dark offset does not arise from the Earth reflection but is an intrinsic instrument offset and has therefore to be subtracted. The effect of the sun-earth distance is considered by the factor *f*; finally, the cosine of the solar zenith angle corrects the different illumination conditions at the top of atmosphere introduced by different solar altitudes.
The effective cloud albedo is then derived from the normalized pixel count ρ, the clear sky reflection $\rho_{srf}$ and the albedo of a compact (not convective) cloud deck $\rho_{max}$ by

$$n = \frac{\rho - \rho_{srf}}{\rho_{\max} - \rho_{srf}} \qquad \text{Eq. 4-4}$$

Here, ρ is the observed reflection for each pixel and time. $\rho_{sfc}$ is the clear sky reflection, which is a monthly value determined for every pixel separately. In principle this is done by estimation of a minimum reflection during a certain time span (e.g., a month) derived for each pixel of the satellite image, please see Posselt et al. (2011) or Posselt et al (2012) for further details. $\rho_{\max}$ is the "maximum" cloud albedo. It could be determined in a similar fashion by choosing the "maximum" ρ per pixel and time span (Beyer et al., 1996) or by using a single value for the full disk that is dependent on the radiometer of the different satellites (Hammer et al., 2003). MAGICSOL follows the approach of Hammer et al. (2003) but a target region is used instead of the whole disk. One value of $\rho_{\max}$ is retrieved for each month, please see section 4.2.3 for further details.

The effective cloud albedo is related to the solar irradiance via the clear sky index. The clear sky index is defined as

$$k = SIS / SIS_{CLS} \qquad \text{Eq. 4-5}$$

which transforms to Eq. 4-6 for spectrally resolved irradiance:

$$k^{wb} = SIS^{wb} / SIS^{wb}_{cls} \qquad \text{Eq. 4-6}$$

Here SIS is the all sky solar surface irradiance and $SIS_{cls}$ is the clear sky irradiance, the term $^{wb}$ denotes that tie radiation is given for wavelength bands.

The relation between the effective cloud albedo CAL and the clear sky index is mainly given by (Hammer et al., 2003, Posselt et. al, 2011):

$$k = 1 - CAL \qquad \text{Eq. 4-7}$$

This relation is defined by physics, in detail by the law of energy conservation (Dagested, 2005). However, above a CAL value of 0.8 empirical corrections are needed in order to consider:

- The effect of statistical noise, which could lead to CAL values above 1 and below 0 (occurs very seldom, however have to be considered).
- The effect of optical thick convective clouds.

In this regions the k-CAL relation was determined from the statistical regression using the ground-based measurements at European sites and fitted to get the best performance at all the ground sites (Hammer et al. 2003 and references therein). Eq. 4-8 provides the complete Helisoat relation for all possible CAL values. It is important to note that the empirical fit has been performed in the 80s and used since then without refitting. The RMSD of the empirical fit is 0.1.

$$CAL < -0.2, \quad k=1.2, \qquad \text{Eq. 4-8}$$
$$-0.2 \le CAL \le 0.8, \; k = 1 - CAL,$$
$$0.8 < CAL \le 1.1, \; k = 2.0667 - 3.6667 * CAL + 1.6667 * CAL^2,$$
$$1.1 < CAL, \; k = 0.05$$

As a consequence of the definition of the clear sky index, the surface solar irradiance for the full-sky situation is given by,

$$SIS = k * SIS_{CLS} \qquad \text{Eq. 4-9}$$

For spectrally resolved irradiance this transforms to

$$SIS^{wb} = k^{wb} * SIS^{wb}_{cls} \qquad \text{Eq. 4-10}$$

where $SIS_{cls}$ is the broadband and $SIS^{wb}_{cls}$ is the spectrally resolved clear-sky solar surface irradiances, broadband and calculated using the MAGIC code (Mueller et al., 2004, 2009), described in section 4.1.

The source code of the method (Mesoscale Atmospheric Global Irradiance Code – MAGIC) was developed externally and is available under gnu-public license free of charge at http://sourceforge.net/projects/gnu-magic/.
Surface solar irradiance data sets derived with the Heliosat method and relation (e.g. Eq. 4-8) have been extensively validated against the ground-based solar radiation measurements (Perez et al., 2001; Wald et al., 2002; Meyer et al., 2003; Rigollier et al., 2004). It is well recognized that the surface solar irradiances derived from satellite measurements can be more accurate than that interpolated from the ground-based measurements, which are more than 30 kilometers apart (Perez et al., 1997; Zelenka et al., 1999). The validation results have demonstrated that the SIS-CAL relation is quite robust.

The occurrence of clouds results in a shift of clear sky spectrum from the red towards the blue range. Hence, a conversion from the broadband cloud transmission described by the clear sky index k to a wavelength dependent transmission $k^{wb}$ is required.
The clear sky state does pre-dominantly not effect the spectral correction discussed hereafter. Hence the standard atmosphere of the basis LUT has been used for the derivation of the spectral correction. In order to derive the spectral correction of the effective cloud albedo, libRadtran RTM runs have been performed for SAL=0 and SZA=0 for cloud layers with cloud optical depth values of COD=0, 10, 20, 40, 80 and 160 for the different wavelength bands and for the broadband. The corresponding wavelength dependent clear sky index values are gained through division of the resulting solar surface irradiance by the irradiance for COD=0. Hence clear sky indices for all wavelength bands and the broadband are available after this step. The broadband clear sky index values for the different CODs are
k=1, 0.525, 0.244, 0.197, 0.102 and 0.050, respectively.
Conversion factors are calculated for each wavelength band $k^{wb}$ with the radiative transfer model by application of Eq. 4-5 in order to consider the spectral effect of clouds on the broadband transmission.

$$f^{wb} = k^{wb}_{RTM} / kb_{RTM} \qquad \text{Eq. 4-11}$$

Here $k^{wb}_{RTM}$ and $k_{RTM}$ are the wavelength band and broadband clear sky index values, respectively calculated with the RTM libradtran for different cloud optical thickness.

The resulting conversion factors are shown in Figure 4–3. These conversion factors are saved in a LUT and applied to correct the wavelength effect of clouds on the clear sky transmission for every satellite pixel and time. Therefore the spectrally resolved irradiance is derived by multiplication of the conversion factors $f^{wb}$ with the broadband clear sky index derived from satellite images by application of Eq. 4-12

$$k^{wb}_{sat} = f^{wb} * k^{sat}_{(CAL)} \qquad \text{Eq. 4-12}$$

The spectrally resolved irradiance is finally derived by application of Eq. 4-13

$$SIS^{wb} = k^{wb}_{sat} * SIS^{wb}_{cls} \qquad \text{Eq. 4-13}$$

The surface reflection is already accounted within the retrieval of the effective cloud albedo which motivates the setting of the surface albedo to zero. However, the effective cloud albedo is retrieved with a broadband visible channel, hence, the spectral dependency of multiple scattering between clouds and the surface is not accounted for within the applied spectral correction.

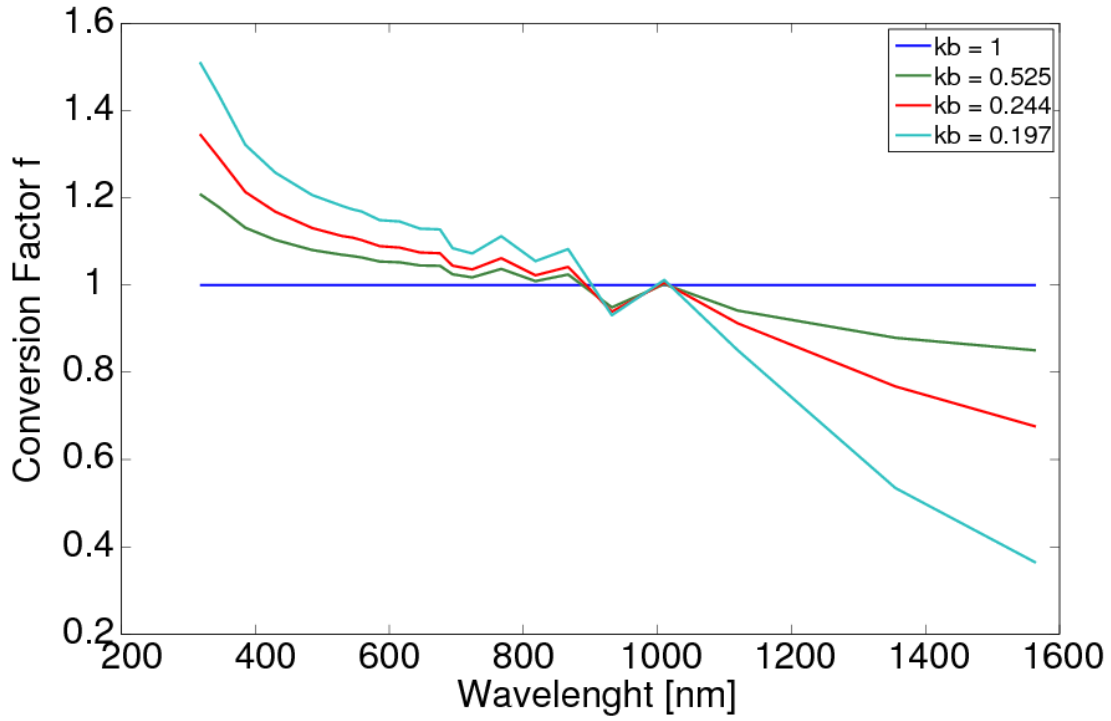


Figure 4–3: The conversion factors for the spectral resolved effective cloud albedo.

### 4.2.3 Auto calibration

For a climate data set homogeneity is an essential issue. Hence, there is a need for "calibration". In this section the auto-calibration method is described and evaluated.
The self-calibration algorithm is based on an operational determination of the "maximum" effective cloud albedo $\rho_{max}$. Input is sun zenith angle normalised counts corresponding to Eq. 4-3.
In analogy to Rigollier et al. (2002) a histogram of all available counts is generated. However, instead of using an upper and a lower bound, only the 95%-percentile is used as self-calibration parameter and set to $\rho_{max}$ (Hammer et al, 2003 and references therein).
However, the generation of the histogram for the full disk is rather slow due to the large pixel amount. Thus, a reduction of the considered region for the histogram was necessary. The selected region is located in the southern ocean between 15° W and 0° W and 58° S and 48° S. It features a high abundance of frontal systems with large cloud amounts most of the time, but hardly any convection.
A range of percentiles has been tested and the 95 percentile has been found to provide the best statistical stability. Using a percentile value and not the maximum of the histogram should exclude saturated pixels, which may have technical but no scientific reasons, and it also should exclude potential convective clouds. Depending on the applied method deep convective clouds might be useful for calibration, but they affect the stability of the 95 percentile applied within the MAGICSOL method
The self-calibration algorithm is run at the 13 o'clock slot GMT which accounts for the slight

westward shift of the region. The histogram is generated with a month worth of satellite data input. The resulting $\rho_{max}$ is then applied for all slots within that month.
Figure 4–4 shows the temporal evolution of the normalized bias between the CM SAF data set and the BSRN data. The normalized difference is calculated as follows:
The arithmetic average over the complete time series of the BSRN and the satellite data is calculated for each station. The resulting mean difference (bias) is subtracted from all monthly means of the satellite data for each station. The mean difference (bias) over the covered time period is zero afterwards; however, **trends in the monthly differences are not affected by this normalization procedure**.
The differences between the monthly means of BSRN and satellite data are then averaged over all available stations, whenever monthly means from at least 3 stations are available. This leads to an overall time series of “normalized” differences of monthly means. This time series is then analysed for temporal trends. A trend in this time series would indicate in-homogeneities introduced by the self-calibration or the clear sky reflection maps. The applied method is necessary in order to avoid misleading trends in the monthly differences introduced by the quite different start and end points of the time series and the corresponding mismatch in the weighting of regional bias values. For the test of the self-calibration it is necessary to avoid artefacts due to local bias values as only the temporal evolution of the time series for the complete disk is of relevance. Contrary, the temporal evolution of the normalised mean monthly differences is not affected by the different numbers of available stations for certain months and their local bias:
As can be seen there is no detectable trend in the temporal evolution of the normalized monthly differences, which proves evidence of the homogeneity of the SIS time series. In contrast, the satellite raw counts show a significant and large trend, a decrease of the sensibility due to aging, see Figure 4–5. The absence of this trend in the normalized differences of the SIS data demonstrates the ability of the self-calibration method to correct for aging and satellite switches.
It is worth noting that a statistically significant negative trend in the normalized differences is present in the GEWEX and ISCCP SIS data sets.

Because the Heliosat method is dedicated to retrieve the effective cloud albedo, a "clear sky" surface target has been not implemented for the self-calibration. Using a land surface target would introduce errors in the self-calibration method as the aging detected by observation of surface reflection is different to that detected with an appropriate cloud target. This is due to the stronger aging of optical devices in the UV and UV-near spectral regions, which leads to different rates of aging for the various land surface types (due to different spectral responses of the targets) in relation to clouds. Every aging of “clear sky" reflection for the different surface types is automatically accounted for by the retrieval of the planetary clear sky reflection (in counts) $\rho_{srf.}$

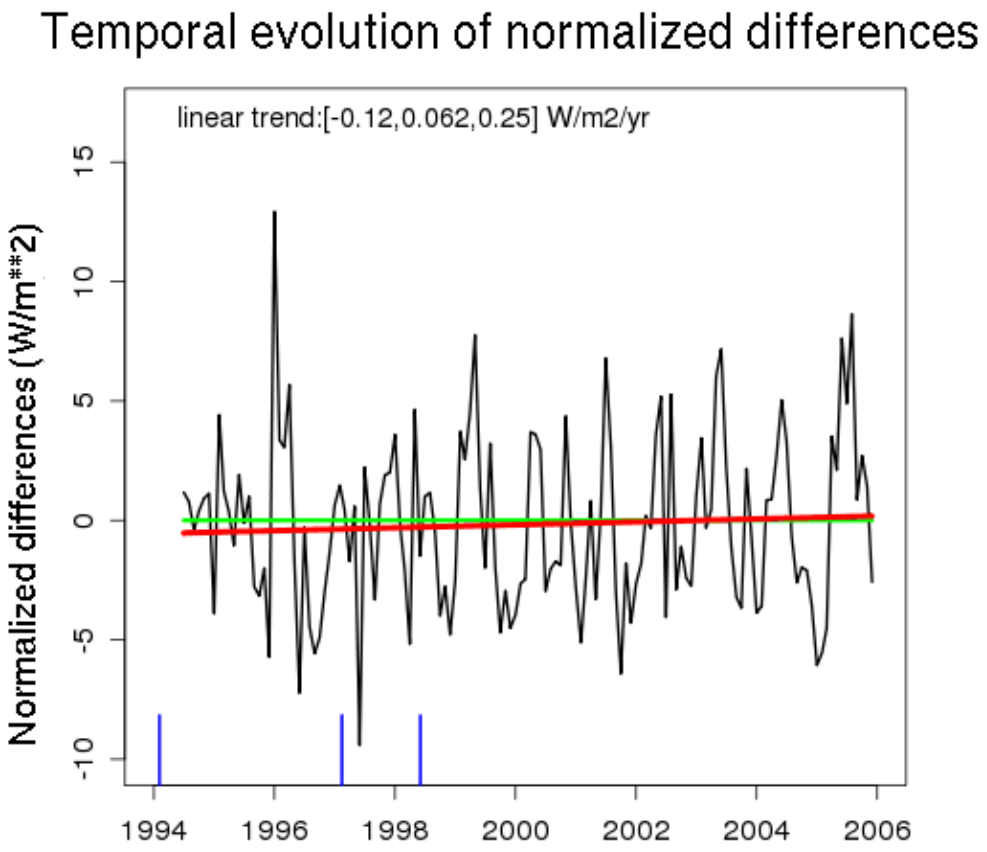


Figure 4–4: Temporal evolution of the normalized differences between the CM SAF data set and the BSRN data including the trend coloured in red. The trend is not significant, both concerning the statistical significance and the magnitude. The absence of a trend in relation to the large trends in the digital satellite counts (Figure 4–5) demonstrates that the self-calibration works well.

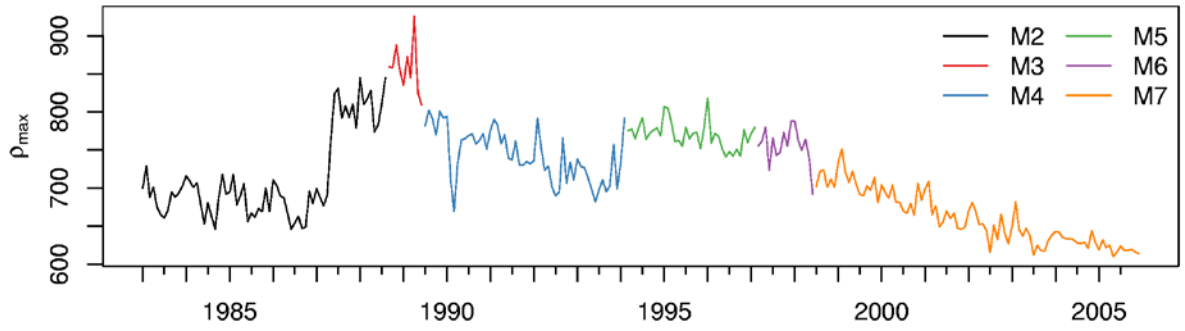


Figure 4–5: Time series of $\rho_{max}$ from 1983 to 2006. The different colours are assigned to the different Meteosat satellites M2_M7 as given in the legend. Meteosat-1 data quality is to worse to be used for the data set. The jump around 1987 within the M2 time series is due to a gauge change of the instrument, performed by the Eumetsat ground segment. The gauge jump has been well detected and corrected by the self-calibration method as well as the large instrument degradation given for Meteosat-7 (see validation report).

### 4.2.4 Averaging

Monthly, daily and hourly means are calculated by arithmetic averaging, using:

$$SRI_{mean} = \frac{\sum_{i=1}^{n} SRI_i}{n} \qquad \text{Eq. 4-14}$$

Here is a loop over the slots per hour for the calculation of hourly means, a loop over the hourly means for the calculation of the daily means and a loop over daily means for the calculation of monthly means.
SRI is either the i-th daily mean for the calculation of the monthly mean or the i-th hourly mean for the calculation of the daily means. Only the finite values of CAL are summed up, n is the total number of finite values. The larger the number of available images per day, the better the daily cycle of cloud coverage can be resolved, increasing the accuracy of the daily average of SRI. A minimum number of three available pixels per day are required to derive the daily mean for this specific pixel. The monthly average is calculated from the daily means of this month on pixel basis as arithmetic mean with a required number of 10 existing daily means. The hourly means are calculated as arithmetic average using Eq. 4-14

### 4.2.5 Atmospheric input information

Here the atmospheric input information used to retrieve the solar irradiance SIS and SID is described. The sensitivity of these parameters on the direct irradiance is discussed in section 4.2.6:

***Effective cloud albedo and clear sky index:***
The effective cloud albedo and clear sky index are derived with the MAGICSOL method; see section 4 for further details.
The effective cloud albedo is taken from the released CM SAF MVIRI data set (Posselt et al., 2011) and will be calculated from CM SAF GERB/SEVIRI top of atmosphere albedo for the time period covered by SEVIRI.

***Aerosol:***
Aerosols have a significant effect on the solar irradiance. They scatter and absorb solar radiation. In order to describe the effect of scattering and absorption, information about the aerosol type and aerosol optical depth is needed. The aerosol type determines the relation between scattering and absorption. This relation can be expressed in terms of the single scattering albedo. The asymmetry parameter depends also on the aerosol type (size and composition) and determines the relation between forward- and backward-scattering. However, for the calculation of direct irradiance only the aerosol optical depth is relevant, as the AOD is defined as the attenuation of direct irradiance. The aerosol type and hence the single scattering albedo and asymmetry factor are only of relevance for the total solar irradiance (diffuse + direct irradiance) and thus for the relation between direct and total solar irradiance for a given AOD (please see section 4 for details)
Monthly mean aerosol information is taken from the aerosol climatology by Kinne et al. (2005), which is based on AEROCOM (http://dataipsl.ipsl.jussieu.fr/AEROCOM/) model median and AERONET ground based measurements. This climatology is available in a 1x1 degree resolution and monthly long term means. It has been evaluated to outperform the GADS/OPAC (Hess et al., 1998) climatology in Africa (Ineichen, 2010) where ground measurements are very rare.

***Water vapour:***
Water vapour is an important absorber. It does not scatter solar radiation and its attenuation effect is pre-dominantly independent on the underlying aerosol state.

Monthly values of integrated water vapour are taken from the global reanalysis data set of ECMWF (ERA-40 and ERA-Interim) Total water vapour from the ERA-interim Reanalysis have been used from 1989 onwards. Up to 1989 ERA Reanalysis data have been used (Uppalla et al., 2005 anmd Betts et al. 2009). Monthly means are on 0.5x0.5 degree latitude-longitude grid. The pixel value is derived by spatial interpolation and assignment of the respective monthly mean.

***Ozone:***
Ozone is a strong absorber in the UV but the absorption is quite weak within the broadband spectrum which is relevant for the estimation of the direct irradiance.
For ozone the climatological values from standard atmosphere are used (Krämer et al., 2003).

***SAL:***
As a database for spectral reflectance we use the spectral response functions assigned to each of 20 land-use types, originating from the NASA CERES/SARB Surface Properties Project, Loveland et al. (1997) and Brown et al. (1993).
The spectral resolution equals the grid of the correlated-k Fu/Liou parameterization in the range of 800-4000nm. Within the 290-800nm range the albedo files provided with libradtran can be used, which have a significant higher spectral resolution. These are not defined for the same land-use types, but for a smaller set of classes like lawn, grass, water and rye.
To solve this problem we use a feasible linear combination of libRadtran spectral reflectance to estimate the reflectivity of the NASA CERES/SARB classes. The diurnal variation of the spectral surface albedo is determined as a function of solar zenith angle, as given by Dickinson et al. (1983). The scene dependent solar zenith adjustment factors needed for this function are also taken from the NASA CERES/SARB Surface Properties Project.

### 4.2.6 Uncertainty estimates

This section provides the uncertainty or sensitivity of SRI induced by the input parameters. The error and accuracy of SRI is assessed by comparison with in-situ data and provided within the validation report. Beside the effect of the clear sky index, aerosols and water vapour have a significant effect on the attenuation of the solar irradiance in cloud-free cases, while the surface albedo effect is rather weak. For all sky cases clouds have also a significant effect on the spectrum.

#### 4.2.6.1 Water vapour

Figure 4–6 provides the sensitivity of the solar surface irradiance SIS on water vapour. The deviation of the direct irradiance is plotted against water vapour variations relative to 15 mm (~ value of the USS standard atmosphere). The sensitivity depends on the solar zenith angle, the total amount of water vapour and the spectral band. The sensitivity is much higher for low water vapour amounts.

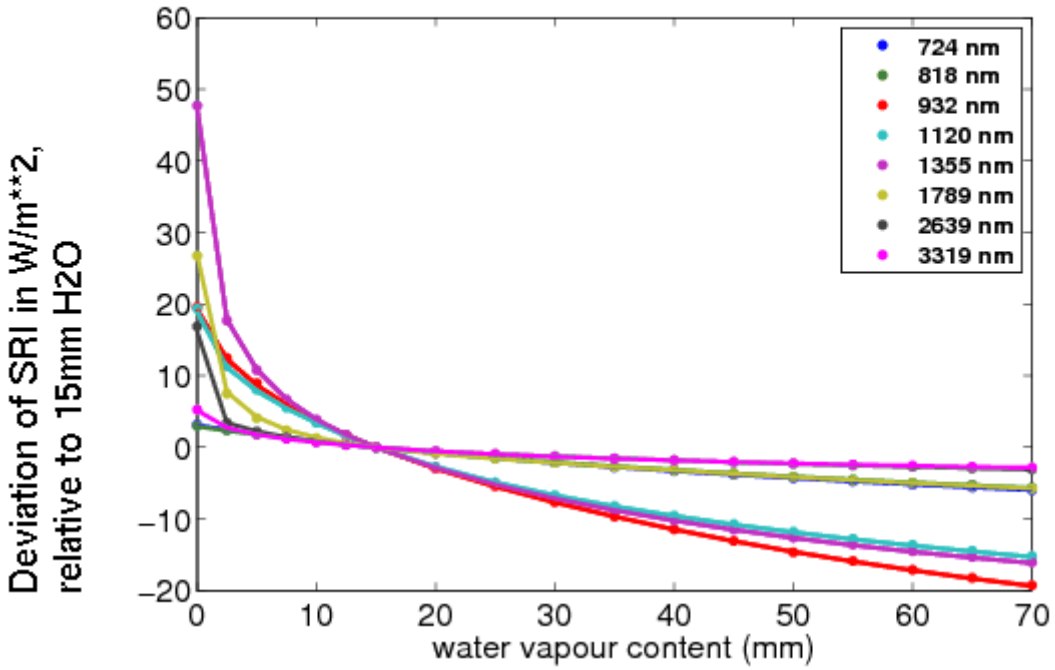


Figure 4–6: The sensitivity of spectrally resolved irradiance SRI on water vapour variations for different wavelength bands at a SZA of 20°.

#### 4.2.6.2 Ozone

Figure 4–7 provides the sensitivity of SRI on ozone. The deviation of SRI is given in dependency of ozone variations relative to 345 DU (~ value of the USS standard atmosphere). The sensitivity depends on the solar zenith angle and is quite small throughout the ozone range. The deviation of direct irradiance is about 1 W/m² for typical ozone variation (+/-100 DU) within the SEVIRI disk. Again the sensitivity of the solar irradiance on ozone is slightly higher than that given for the direct irradiance.

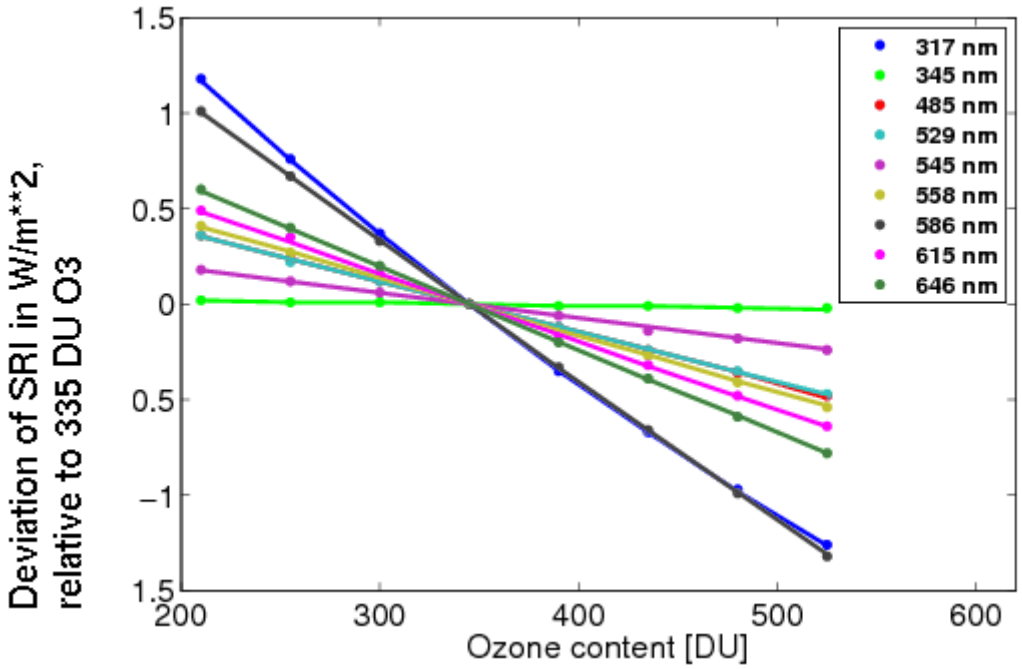


Figure 4–7: The sensitivity of solar irradiance to ozone in different spectral banes and for a SZA of 20 degree.

#### 4.2.6.3 Aerosols

Aerosol type, expressed as single scattering albedo and asymmetry parameter, has a significant effect on the solar irradiance and determines the relation between solar irradiance and direct irradiance. The single scattering albedo describes the relation between scattering and absorption, while the asymmetry parameter describes the relation between forward and backward scattering (as a consequence of the particles size). The sensitivity of the aerosol information on the broadband irradiance has been already discussed in RD.1. Here, we focus on the affect of aerosols on the spectrum which is a consequence of different aerosols types in particular the size of the particles, and the amount of soot. Figure 4–8 shows the effect of different aerosol types on the solar spectrum as derived with the radiative transfer model libRadtran. As can be seen the spectral sensitivity is rather week, only for urban aerosols a significant effect in the range of 350-700 nm occurs.

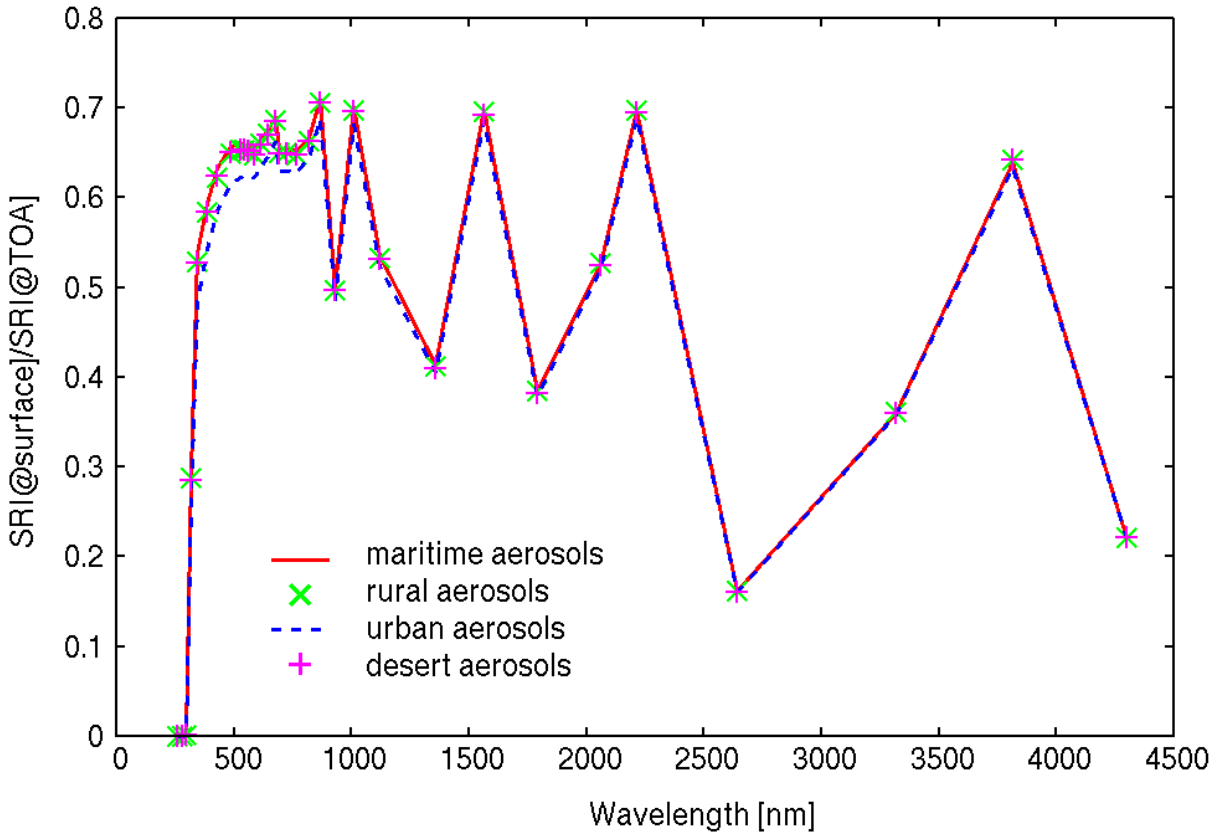


Figure 4–8: Sensitivity of spectrally resolved irradiance in the aerosol type.

#### 4.2.6.4 Surface albedo

The spectral sensitivity depends on the spectral response function of the assumed surface types. Figure 4–10 illustrates the spectral response of different surface types on the solar irradiance. Variations in SAL in each wavelength band leads to a linear change in the solar irradiance corresponding to Eq. 4-2. Figure 4–10 illustrates the sensitivity on SAL which is equal in each wavelength band. Deviations of +/- 0.1 in the spectral surface albedo lead to deviations in clear sky SIS of +/- 1%. The effect is almost linear. Errors in the surface albedo are expected to be typically less than 0.1, with exception of snow covered surfaces, where higher errors might occur. The effect is pre-dominantly independent on the clear sky atmospheric state.

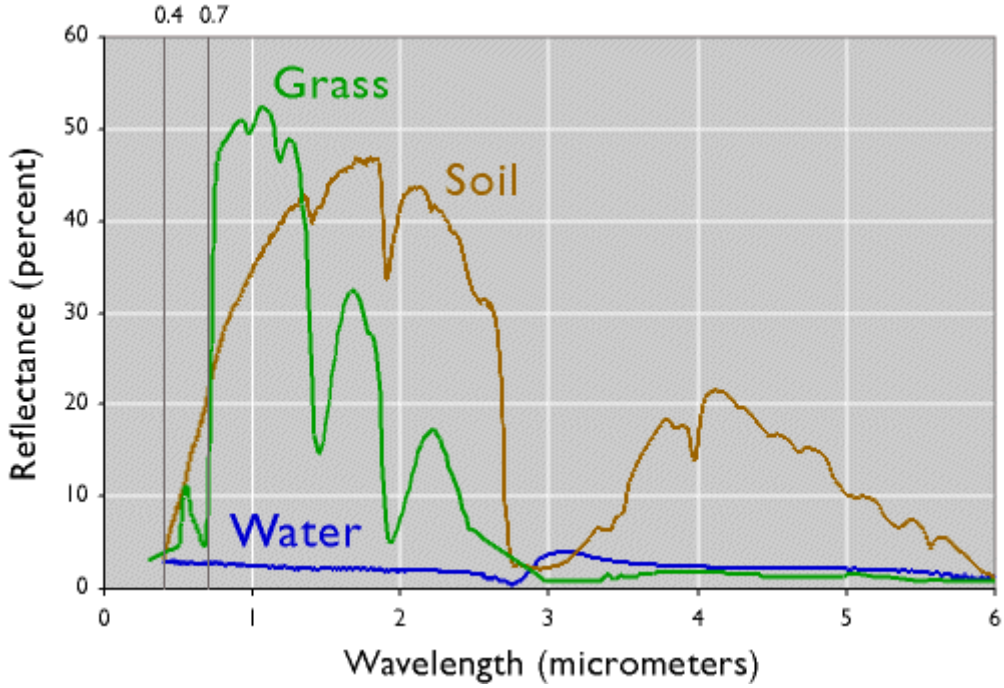


Figure 4–9: Example of the spectral response of different surface types, here for grass (vegetation) soil and water.

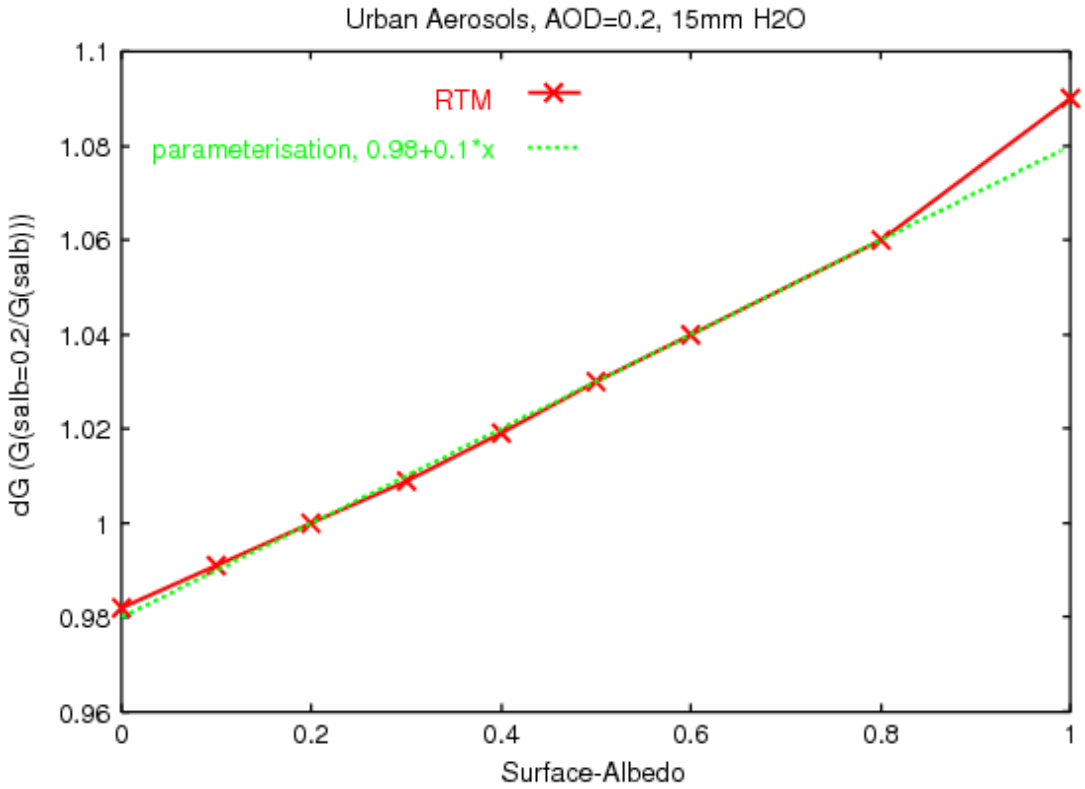


Figure 4–10: Sensitivity of the solar irradiance SRI on the surface albedo. The red line shows the RTM results and the green line the applied parameterisation. The horizontal axis shows the deviation of SRI with variable surface albedo relative to SRI calculated for a fixed surface albedo of 0.2. For deviations of +/- 0.1 in the surface albedo the uncertainty in SIS is +/- 1%. With exception of values above 0.9 the parameterisation matches the RTM results quite well.

#### 4.2.6.5 Sensitivity of CAL on self-calibration method

The effective cloud albedo is defined as a relative quantity of observed counts or radiances. Hence, any noise or uncertainty in the satellite observations is predominantly cancelled out. The uncertainty in the effective cloud albedo is therefore pre-dominantly determined by uncertainties in the determination of the clear sky reflection and the self-calibration method.

The uncertainty or fuzziness in $\rho_{\max}$ defined by the month to month variations of $\rho_{\max}$ is in the order of 3%. However, it is likely that part of this uncertainty is due to local biases in the satellite counts and not due to errors in the retrieval of $\rho_{\max}$. Local biases of the satellite counts would transfer to equal relative amounts into $\rho_{\max}$ and $\rho_{srf}$, and would be therefore pre-dominantly cancelled out within the calculation of the effective cloud albedo (Figure 4–11), Hence, they would not affect the accuracy of CAL. However, as it is not possible do estimate to which amount the local biases counts to the $\rho_{\max}$ uncertainty the complete uncertainty is assumed to arise from the applied statistical retrieval method. This is a worst case approach, since the uncertainty given by the $\rho_{\max}$ retrieval method is likely significantly smaller than 3% and hence also the effect of the $\rho_{\max}$ retrieval method on the accuracy of CAL. The $\rho_{\max}$ uncertainty is constant in terms of relative uncertainty throughout the cloud index interval, but different for different surface types. Figure 4–11 shows the effect of a 3 % uncertainty on $\rho_{\max}$ on the effective cloud albedo in absolute values. For a CAL value of 1 the absolute value is equal to the relative uncertainty, which is constant throughout the CAL range.

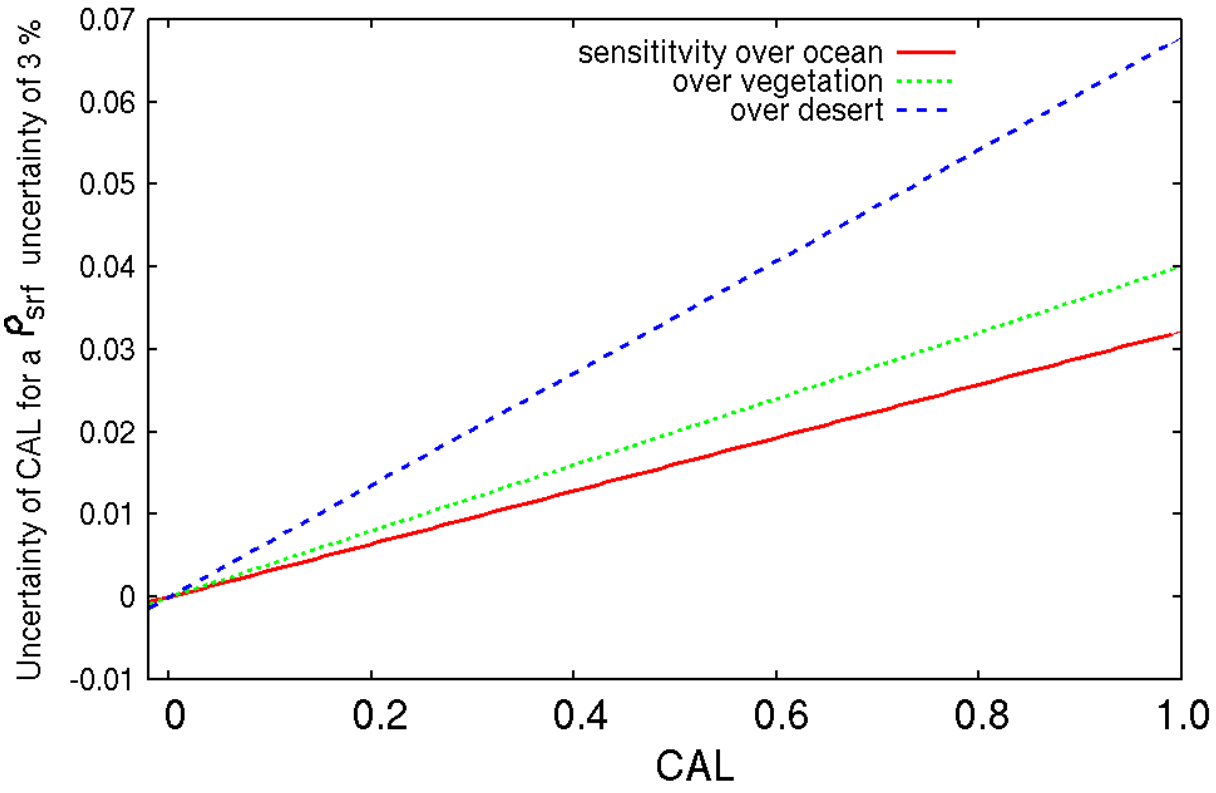


Figure 4–11: Sensitivity of the effective cloud albedo on the $\rho_{\max}$ uncertainty for different surface types, with an albedo of 0.05 (~ocean), 0.15 (~vegetation) and 0.35 (~desert).

#### 4.2.6.6 Sensitivity of CAL on clear sky reflection

Figure 4–12 shows the effect on uncertainties in the clear sky reflection on the effective cloud albedo. The effect is rather weak, as a consequence of the occurrence of $\rho_{srf}$ in the dominator and nominator of the effective cloud albedo formula. However, the clear sky reflection introduces significant uncertainty and error in the effective cloud albedo retrieval for the case of cloud contamination. This happens if not enough clear sky cases occur. Hence, for regions with long-lasting cloud cover in combination with slant geometry the $\rho_{srf}$ retrieval fails to see the clear sky situations, hence $\rho_{srf}$ is contaminated by clouds and is artificially increased, see Figure 4–13. This effect occurs pre-dominantly at the border of the MFG disk, above 60 degrees, see Figure 4–14. As it occurs only for regions with long-lasting cloud coverage (hence large values of the effective cloud albedo) the effect on the solar irradiance is much lower as implied by the uncertainty in the effective cloud albedo.

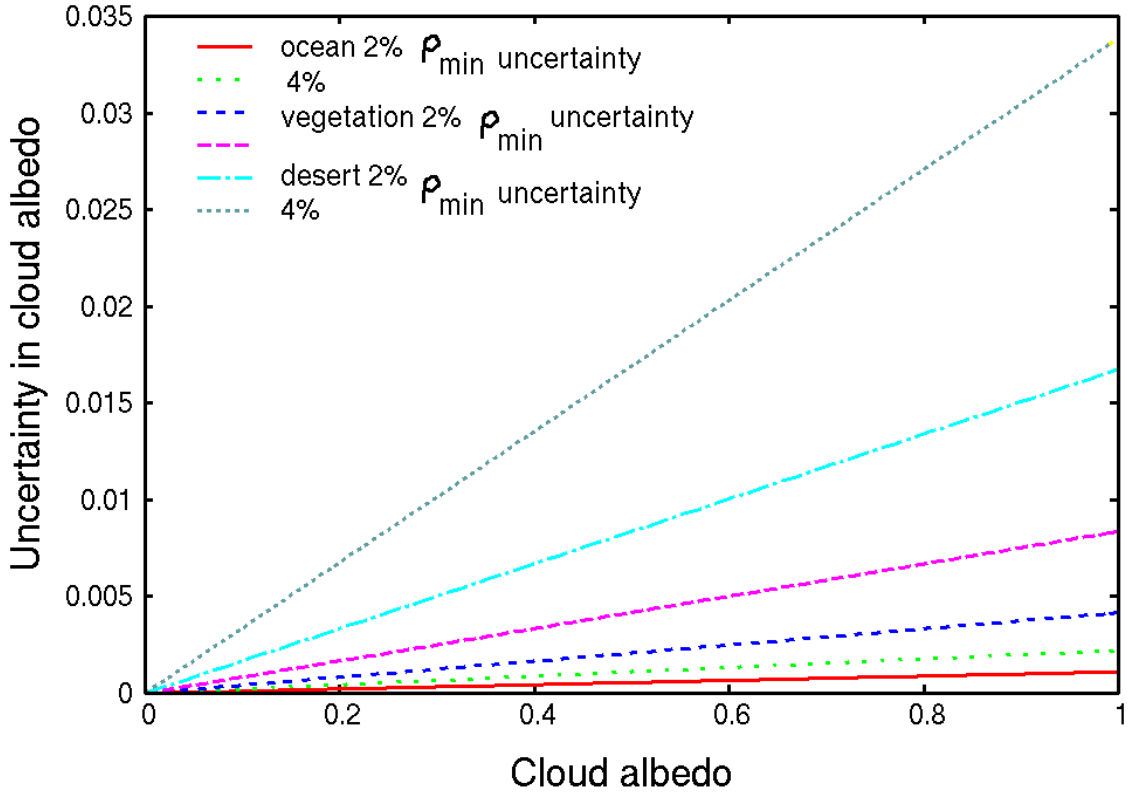


Figure 4–12: Sensitivity of the effective cloud albedo on the clear sky reflection $\rho_{srf}$ . The x-axis compiles the range of the cloud index. On the y-axis the uncertainty or error of the effective cloud albedo is given for different surface types and uncertainties in the retrieval of $\rho_{srf}$ of 2% and 4%, respectively, arising from “statistical noise”. The effect of uncertainties of $\rho_{srf}$ on the effective cloud albedo is rather weak. Only for desert (sand) surface an errors in the retrieval of $\rho_{srf}$ would lead to significant errors in the effective cloud albedo.

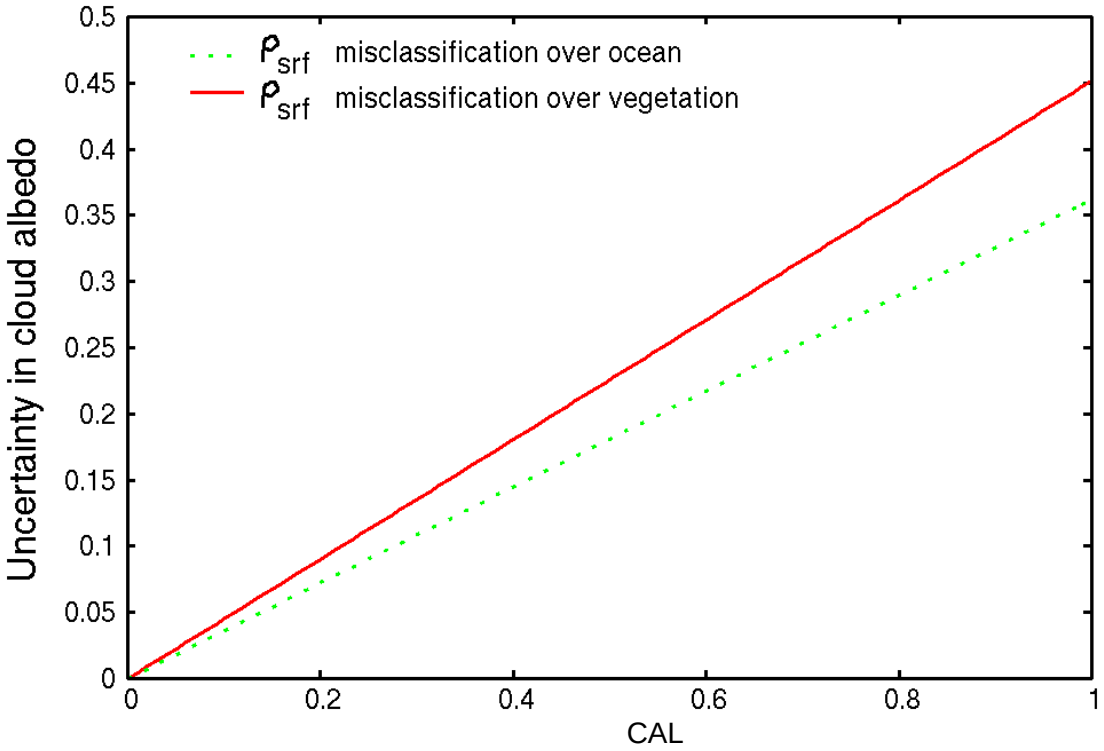


Figure 4–13: Effect of cloud contamination of clear sky reflection on the effective cloud albedo. The effect is rather large. However it occurs pre-dominantly at the border region of the MFG disk. Further on, the effect occurs for long-lasting cloud coverage, the resulting higher uncertainty in the effective cloud albedo has therefore a relative small effect on SIS.

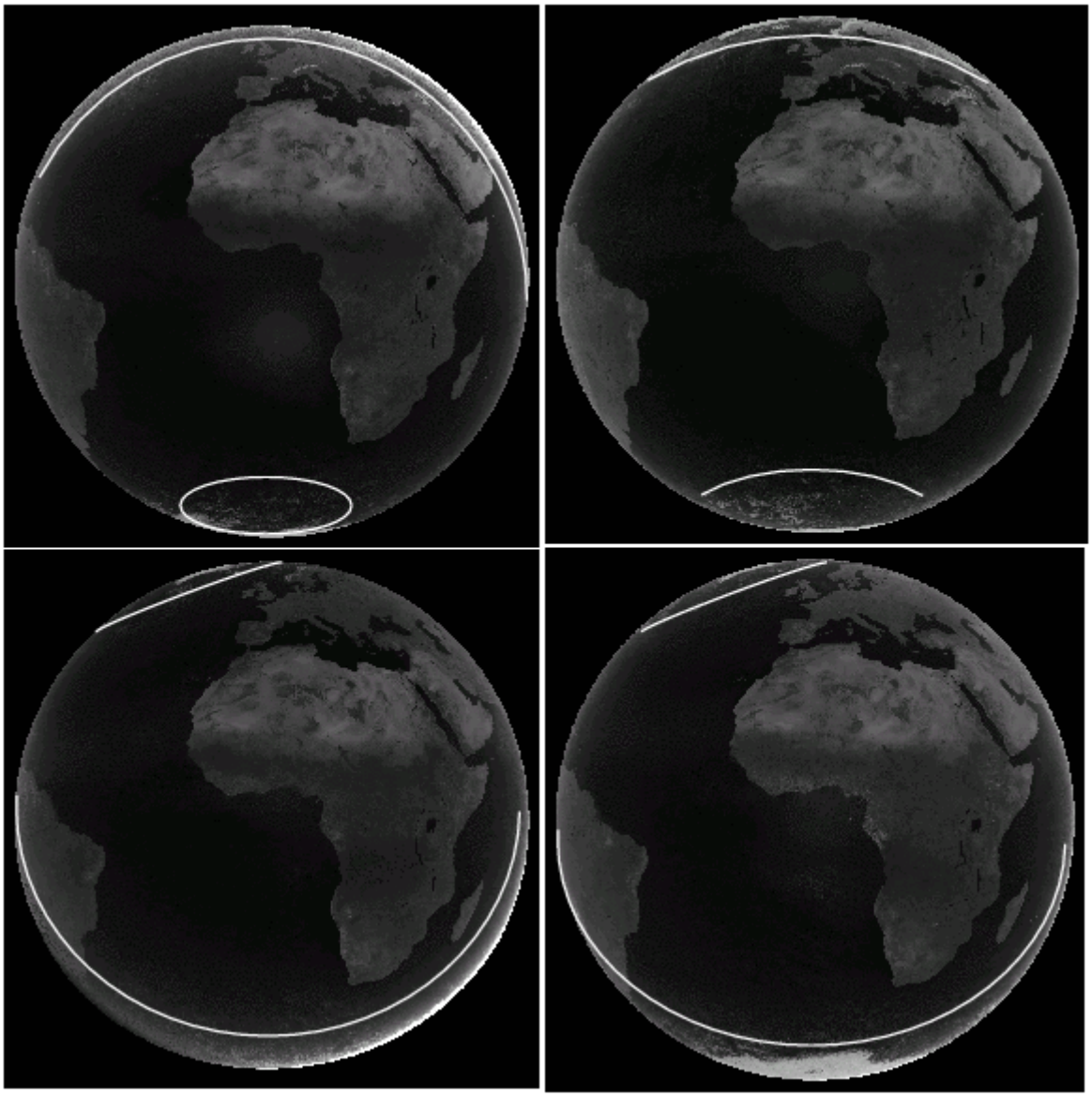

**Figure 4–14:** Examples of $\rho_{sfc}$ images, here for 2000, 12 GMT, from top left to bottom right, December, March, June and September. The white speckle patterns beyond the white lines close to the border of the disk are due to significant cloud contamination of $\rho_{sfc}$ .However, close to the poles, some white regions are not an artefact bur due to ice (Greenland & Arctic in the September image). Cloud contamination occurs also in a small band around sunrise and sunset at the East and West border of the disk, respectively. However, the core of the Meteosat disk is almost not affected.

## 4.3 Practical considerations

### 4.3.1 Calibration, Validation and Quality control

Calibration is performed by the auto-calibration method described in detail in section 4.2.3. Validation (quality control) will be performed by comparison with ground measurements and will be presented and discussed in the validation report. At this stage the maturity of the algorithm can only be evaluated by comparison with explicit radiative transfer model results.

Figure 4–15 shows the comparison of the method discussed with the output of radiative transfer model (Mueller et al. 2004). The differences are below of 1 % throughout the spectral range. Note, that the application of an RTM is a very slow path which limits the application for the calculation of SRI for long time series with a large geographical coverage. Hence, retrieval algorithms are inevitable for practical purposes like the satellite based retrieval of spectrally resolved irradiance.

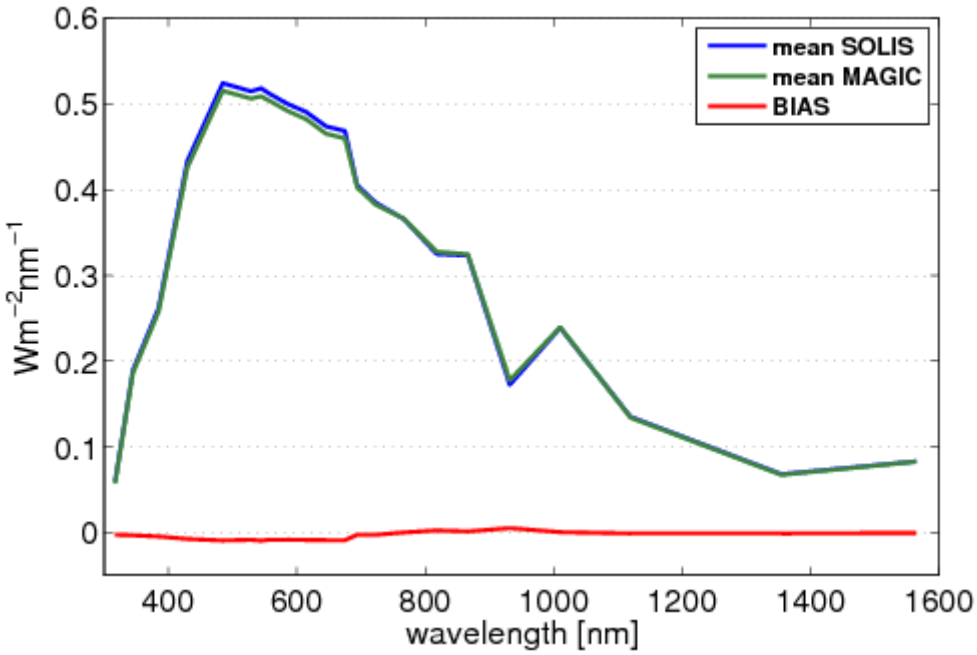


**Figure 4–15:** Average spectrum for Kato bands retrieved with MAGIC (spectral version) and with SOLIS for typical atmospheric conditions in Europe. The bias is given as red line in addition.

### 4.3.2 Outputs

The output of the algorithm will be spectrally resolved irradiance in 32 Kato bands.

## 5 Assumption, limitations and future improvements

- The high clear-sky reflection over bright surfaces (e.g., desert regions) reduces the contrast between clear-sky reflection and cloudy-sky reflection. This leads to higher uncertainties in CAL and errors in the calculation of SRI.
- In regions with long-lasting cloud cover the detection of a minimum which constitutes a clear sky situation might fail. This results in an underestimation of the effective cloud albedo and errors in SRI.
- The accuracy of aerosol information is unknown in several regions of the world due to missing ground measurements. Any uncertainty in the aerosol information affects the accuracy of SRI, especially in regions that are dominated by cloudless sky.
- For the calculation of the look-up tables of the clear sky model standard ozone and aerosol profiles are used. These profiles are scaled with the respective vertical column values; see Mayer and Kyling (2005) for further details.

- The USS standard atmosphere has been used to consider the effect of air molecules (e.g. Rayleigh scattering). However, this has no effect on accuracy (Mueller et al, 2009)
- The anisotropy of the cloud reflection leads to uncertainties in the effective cloud albedo and subsequent in the solar surface irradiance. The respective effect is in the order of 1 to 2 % for monthly and daily means respectively. An improved correction of the anisotropy effect will be developed for the next release. However, in general the anisotropy effect is rather small.
- The self calibration method in combination with the modified retrieval of $\rho_{srf}$ is sensible to significant changes in spectral channels. This implies that using the VIS006 or the VIS008 channel of MSG instead of the broadband channel will lead to significant differences in the effective cloud albedo in specific regions (please see Posselt et al, 2011 for further details). The item is not relevant for the discussed MVIRI climate data sets herein but for the planned prolongation of the record by the use of SEVIRI on board of MSG.
- It is assumed that the radiative transfer model does provide accurate information about the cloud effect on the solar clear sky spectrum

# 6 References

Betts Alan K., Martin Köhler and Yuanchong Zhang, 2009: Comparison of river basin hydrometeorology in ERA-Interim and ERA-40 reanalyses with observations, Journal of Geophysical Research, Vol. 114, D02101, doi:10.1029/2008JD010761

Beyer, H. G., Costanzo, C., and Heinemann, D.: Modifications of the heliosat procedure for irradiance estimates from satellite images, Solar Energy, 56, 207-212, 1996.

Brown, J.F.; Loveland, T.; Merchant, J.W.; Reed, B.C.; Ohlen, D.O. Using multi-source data in global land-cover characterization: concepts, requirements, and methods. Photogrammetric Engineering and Remote Sensing 1993, 59, 977–987

Cano, D., Monget, J. M., Albuisson, M., Guillard, H., Regas, N., and Wald, L.: A method for the determination of the global solar-radiation from meteorological satellite data, Solar Energy, 37, 31-39, 1986.

Dagestad, K.-F. (2004), Mean bias deviation of the Heliosat algorithm for varying cloud properties and sun-ground-satellite geometry, Theor. Appl. Climatol. 79, 215–224, DOI 10.1007/s00704-004-0072-5
Dagestad K.-F., J. A. Olseth, A modified algorithm for calculating the cloud index (2007), Solar Energy 81, 280–289.

Derrien,M., LeGLeau, H., 2005: MSG/SEVIRI cloud mask and type from SAFNWC. Int. J. Rem. Sens. 26 (21), 4707 – 4732.

Dickinson, R.E. Land surface processes and climate - Surface albedos and energy balance. Advances in Geophysics 1983, 25, 305–353.

Dürr, B., and Zelenka, A.: Deriving surface global irradiance over the alpine region from meteosat second generation data by supplementing the heliosat method, International Journal of Remote Sensing, 5821-5841, DOI 10.1080/01431160902744829, 2009.

Hammer, A., Heinemann, D., Hoyer, C., Kuhlemann, R., Lorenz, E., Müller, R., and Beyer, H. G.: Solar energy assessment using remote sensing technologies, Remote Sens. Environ., 86, 423--432, 2003.

Hess, M.; P. Köpke; I. Schult, 1998: Optical Properties of Aerosols and Clouds: The Software Package OPAC. Bull. Amer. Meteor. Soc., 79, 831-844.

Kinne, S., M. Schulz, C. Textor et al., 2006, An aerocom initial assessment – optical properties in aerosol component modules of global models, Atmos. Chem. Phys., 6, 1815-1834.

Krämer, M., Ri. Müller, H. Bovensmann, J. Burrows, J.-U. Grooß, D. S. McKenna, Ro. Müller, Th. Woyke, J. Brinkmann, E.P. Röth, R. Ruhnke, G. Günther, J. Hendricks, E. Lippert, K. S. Carslaw, Th. Peter, A. Zieger, Ch. Brühl, B. Steil and R. Lehmann, 2003: "Intercomparison of Numerical Stratospheric Chemistry Models under Polar Vortex Conditions". Journal of Atmospheric Chemistry, 45, 51-77.

Loveland, T.; Belward. The IGBP-DIS Global 1 km Land Cover Data Set, DISCover First Results. 508 International Journal of Remote Sensing 1997, 18.
Ineichen, P. “Satellite based short wave irradiance validation over Africa“, Visiting Scientist report of CM SAF, 2010, available at www.cmsaf.eu.

Kato, S., Ackerman, T., Mather, J., Clothiaux, E., 1999. The k-distribution method and correlated-k approximation for a short-wave radiative transfer. J. Quant. Spectrosc. Radiat. Transfer 62.

Köpke, P.; Hess, M.; Schult, I.; Shettle, E., 1997: Global aerosol data set. Tech. Rep., 243, MPI Meteorology, Hamburg.

Koepke, P., Bais, A., Balis, D., Buchwitz, M., de Backer, H., de Cabo, X., et al. (1998). Comparison of models used for UV index calculations. Photochemistry and Photobiology, 67, 657−662.

Mayer, B.; A. Kylling, 2005: Technical note: "The libRadtran software package for radiative transfer calculations - description and examples of use." Atmos. Chem. Phys., 5, 1855-1877.

Mayer, B., Seckmeyer, G., & Kylling, A. (1997). Systematic long-term comparison of spectral UV measurements and UVSPEC modeling results. Journal of Geophysical Research, 102, 8755−8767,

Majewski, D., Liermann, D., Prohl, P., Ritter, B. , Buchhold, M., Hanisch, T., Paul,G. Wergen, W. Baumgardner, J., 2002. The Operational Global Icosahedral–Hexagonal Gridpoint Model GME: Description and High-Resolution Tests, Monthly Weather Review, 130, pp 319.

Möser, W. , 1983: Globalstrahlung aus Satellitenmessungen. Mitteilungen aus dem Institut für Geophysik und Meteorologie der Universität zu Köln, 37, Köln.

Müller, R.W.; Dagestad, K.F.; Ineichen, P.; Schroedter-Homscheidt, M.; Cros, S. Dumortier, D.; Kuhlemann, R. ; Olseth, J.A.; Piernavieja, G.; Reise, C.; Wald, L.; Heinemann,D.; 2004: "Rethinking satellite based solar irradiance modelling – The SOLIS clear sky module", Rem. Sens. Envir., 91, 160-174.

Müller, R.W. et al., 2003-b „Report of the HELIOSAT-3 software package for solar irradiance retrieval, all sky working version" EU report of the Heliosat-3 project (www.heliosat3.de), NNE5-2000-00413

Müller, R.W., Matsoukas, C. Behr, H.D., Gratzki, A. Hollmann, R., 2009: MAGIC - The CM-SAF operational scheme for the satellite based retrieval of solar surface irradiance - a LUT based eigenvector hybrid approach. Accepted for publication in Remote Sensing of Environment,113, 1012-1024.

Posselt, R.; Mueller, R.; Stöckli, R.; Trentmann, J. Spatial and Temporal Homogeneity of Solar Surface Irradiance across Satellite Generations. Remote Sens. **2011**, 3, 1029-1046. Posselt, R.W. Mueller, R. Stöckli, J. Trentmann, Remote sensing of solar surface radiation for climate monitoring — the CM-SAF retrieval in international comparison, Remote Sensing of Environment, Volume 118, 2012.

Rigollier, C., Lefevre, M., Blanc, P., and Wald, L.: The operational calibration of images taken in the visible channel of the meteosat series of satellites, {J. Atmos. Ocean. Technol.}, {19}, {1285-1293}, 2002.

Skartveit, A., Olseth, J., Tuft, M., 1998: An hourly diffuse fraction model with correction for variability and surface albedo. Solar Energy, **63**, 173–183.

Uppala, S., P. Kallberg, A, Simmons, U. Andreae, V. Da Costa Becthold, M. Firion, J. Gibson, J. Haseler, A. Hernandez, G. Kelly, X. Li, K. Onogi, S. Saarinen, N. Sokka, R. Allan, E. Andersson, E. Arpe, M. Balmaseda, A. Beljaars, L. van de Berg, J. Bidlot, N. Bormann, S. Caires, F. Chevallier, A. Dethof, M. Dragosavac, M. Fisher, M. Fuentes, S. Hagemann, E. Holm, B, Hoskins, L. Isaksen, P. Janssen, R. Jenne, A. McNally, J.-F. Mahfouf, J.J. Morcrette, N. Rayner, R. Saunders, P. Simon, A. Sterl, K. Trenberth, A. Untch, D. Vasiljevic, P. Viterbos, J. Woollen, 2005: The ERA-40 reanalysis. – 436 Quarterly Journal of the Royal Meteorological Society 131, 2961 – 3012.

Van Weele, M., Martin, T., Blumthaler, M., Brogniez, C., den Outer, P., Engelsen, O., et al. (2000). From model intercomparisons towards benchmark UV spectra for six real atmospheric cases. Journal of Geophysical Research, 105, 4915−4925.

Zelenka, A.: Estimating insolation over snow covered mountains with meteosat vis-channel: A time series approach, Proceedings of the Eumetsat Meteorological Satellite Data Users Conference, Eumetsat Publ. EUM P, 2001, 346--352,

## 7 Glossary - List of Acronyms in alphabetical order

AVHRR : Advanced Very High Resolution Radiometer
AOD : Aerosol Optical Depth
CAL: Effective cloud albedo
COT Cloud optical depth
CLS: Clear Sky
GADS/OPAC: Global Aerosol Data Set / Optical Properties of Aerosols and Clouds
GERB : Geostationary Earth Radiation Experiment
k: Clear sky index.
LUT: Look-up table
MVIRI : Meteosat Visible-InfraRed Imager
NOAA : National Oceanic and Atmospheric Administration
NCEP: National Centers for Environmental Prediction
RTM: Radiative Transfer Model
SID: Surface Direct Irradiance (beam).
SIS: Solar Surface Irradiance
SZA : Sun Zenith Angle
SSA: Single Scattering Albedo